공학석사학위논문

Analysis of Thermal Conductivity Expressions of Binary Systems near Melting Point using Equilibrium Molecular Dynamics Simulation

녹는점 부근의 2 원계 물질에 대하여 평형 분자동역학 시뮬레이션에서의 열전도율 표현식에 대한 분석

2017 년 7 월

서울대학교 대학원
에너지시스템공학부
류 진 호

Analysis of Thermal Conductivity Expressions of Binary Systems near Melting Point using Equilibrium Molecular Dynamics Simulation

지도교수 **Takuji Oda**

이 논문을 공학석사학위논문으로 제출함.

2017 년 7 월

서울대학교 대학원

에너지시스템공학부

류 진 호

류진호의 공학석사학위논문을 인준함.

2017 년 7 월

위 원 장 황 일 순 (인)

부위원장 **Takuji Oda** (인)

위 원 조 형 규 (인)

Abstract

Analysis of Thermal Conductivity Expressions of Binary Systems near Melting Point using Equilibrium Molecular Dynamics Simulation

Jinho Ryu
Department of Energy Systems Engineering
The Graduate School
Seoul National University

In the field of nuclear engineering, one of the key parameter that governs the temperature of a component device of dielectric materials is the lattice thermal conductivity (TC). However, in the severe conditions of nuclear power plant (NPP) such as high radiation dose, high temperature and pressure, it is quite difficult task to measure or estimate the accurate value of TC of materials composing the devices of NPP during the operation. Therefore, approaches based on the theoretical calculation and simulations has been widely utilized for the estimation of TC under various circumstances.

Among those approaches, the Green-Kubo relations have been considered as a trustworthy method for evaluation of the TC of condensed matters in equilibrium molecular dynamics (MD) calculation. In previous studies adopting the Green-Kubo relations, however, there exist mainly three different expressions of TC, each of which considers a different microscopic phenomenon as the substance of thermal conduction. In the present study, focusing on binary systems, we investigate the theoretical background of the three TC expressions and differences among calculated TC values.

First of all, by deriving the TC expressions from the entropy production equation, we specified the assumptions and conditions employed in each TC expression. This procedure revealed the expression of the least approximation. In addition, three important material properties that affect the differences among the TC expressions are obtained: the Maxwell-Stefan (MS) diffusion coefficient, the partial specific enthalpy, and the reduced heat of transport. MD simulations of Li_2O and TiO_2 systems over a wide temperature range including crystal, amorphous and liquid phases show that when the MS diffusion coefficient exceeds around 10^{-7} cm^2/s, one TC expression exhibits an abnormal value with up to 120% and 60% error compared to the least-approximate TC expression in Li_2O and TiO_2, respectively. Finally, simple method to predict the occurrence of the error based on the self-diffusion coefficient is suggested. This method contains the discussion about the possible advantages and disadvantages of the three TC expressions and about the conditions where a significant error may appear.

Keywords: Thermal conductivity, **Green-Kubo relations, Molecular dynamics, Maxwell-Stefan diffusion coefficient, Heat of transport**

Student Number: 2015-22941

List of Contents

List of Tables

List of Figures

Chapter 1. Introduction

1.1 Importance of the thermal conductivity

In the field of nuclear engineering, the thermal conductivity (TC) of a material is one of the key material's property. For example, the TC of a nuclear fuel governs the core temperature of fuel pellet in relation with the temperature of primary coolant. For safety concerns, the core temperature serves as a limiting criterion in the design of primary system of a nuclear power plant (NPP), that is the nuclear steam supply system (NSSS). If the TC of a nuclear fuel is improved, licensee of NPP would consider increasing the temperature of primary coolant. It will bring considerable amount of economic benefit to the licensee, as the efficiency of heat engine increases at the higher temperature according to the basic theory of thermodynamics. Due to such kinds of importance of the accurate estimation of TC, various experimental and computational methods have been proposed and applied to evaluate TC.

1.2 Methods to evaluate the thermal conductivity

1.2.1 Experimental methods

Among experimental methods to evaluate the TC, the laser-flash technique [1] is currently the most widely accepted method for precise measurement of the TC. With this method, what is measured is the total TC (κ_{tot}), which is composed of electronic and phononic contributions. While the electronic contribution is related to the energy transfer via free electrons, the phononic contribution is related to the energy propagation through the lattice vibration.

If one tries to measure the decomposed TC, the electronic TC (κ_e) can be directly obtained from converting electrical conductivity (σ) using the Wiedemann-Franz law, $\kappa_e = L\sigma T$, where L is the Lorentz number and T is the absolute temperature. However, the lattice TC (κ_{lat}) can only be obtained indirectly in experiments, by subtracting κ_e from κ_{tot}. For ionic and covalent materials where κ_e is usually negligible, κ_{lat} might be approximately considered as κ_{tot}.

1.2.2 Computational methods

Due to the difficulties on the direct measurement of lattice TC, various computational methods have been developed, which is the main topic of this thesis. For the sake of brevity, the lattice TC will be simply noted TC hereafter. Up to the author's best knowledge, there are mainly three distinct methods for the evaluation of TC in calculational methods: Non-equilibrium molecular dynamics (NEMD), equilibrium molecular dynamics (EMD), and lattice dynamics (LD). It is widely known that those three approaches give a comparable result with each other [2], [3], if it were performed appropriately and utilized with appropriate expressions for TC. While the TC expressions in NEMD and LD methods are rather straightforward, if one skims over the published papers, TC expressions in EMD are poorly organized: several different TC expressions appear in EMD.

1.2.3 Objective and approaches of the thesis

Considering the current status of the EMD researches about TC, it is an urgent task to organize the concurrently existing TC expressions in EMD methods. Therefore, the main objective of this thesis is to systematically summarize and evaluate each TC expressions, so as to suggest the best appropriate TC expression among them for the binary systems. In this category of binary systems, quite many systems in practical engineering are involved such as impurity-containing pure metals, metallic oxides, carbides,

hydrides and so on. Therefore, it would benefit related researches corresponds to this category of the binary systems.

To achieve the objective, firstly the theory of non-equilibrium thermodynamics will be revisited to construct a systematic theoretical background for the discussions. Following this theoretical background, each of different TC expressions will be evaluated about its appropriacy starting from the derivation procedure of it. This approach is very fundamental and foundational, thus is expected to give insights about why some of TC expressions are inappropriate, while others are proper.

Secondly, the result of molecular dynamics (MD) calculation of each of different TC expressions will be presented. In combination with our results from the theoretical study in previous section, the result will be interpreted in terms of the properties of material. This interpretation would correspond to several critical questions in this thesis: “Why some TC expression show different value from the others?” and “What is the physical meaning of that difference?”.

Chapter 2. Literature Review

2.1. EMD method for the TC evaluation

As one of the most prevalent method for TC evaluation, the EMD method has been applied to condensed matters including rare gas liquids [4]–[6], covalent crystals [7]–[11], and ionic crystals and liquids [12]–[18]. In an EMD method, the TC is expressed using the combinations of phenomenological coefficient, which relates the phenomenological current and its driving force. For example, if the observed phenomenon is the mass current in a material, then the phenomenological coefficient relates the driving force of mass current (such as the concentration gradient) and the mass current itself. One of the most famous linear phenomenological law would be the Fick's law for the mass diffusion.

2.1.1 The Green-Kubo relation

In an EMD method, the Green-Kubo (GK) relation [19], [20] enables us to calculate a phenomenological coefficient by integration of an associated correlation function, which is described as

$$L_{AB} = \frac{1}{3k_B V}\int_0^\infty \left\langle \mathbf{j}_A(0)\,\mathbf{j}_B(t)\right\rangle dt, \tag{2.1}$$

where L_{AB} is the PC of current A and B, $\boldsymbol{j}_A$ is the current of A quantity, k_B is the Boltzmann constant, and V is the volume of the system. Here, we consider the A quantity as one of various phenomena occurring inside a material. The angled bracket of the integrand denotes the ensemble average of the correlation function, $\boldsymbol{j}_A(0)\,\boldsymbol{j}_B(t)$.

With this phenomenological coefficient, various transport coefficients such as the self-diffusion coefficient, shear viscosity and TC can be evaluated. Among the phenomenological coefficients related to TC, the phenomenological coefficient of the heat current autocorrelation function L_{QQ} is the main component.

2.2. Different TC expressions in EMD method

2.2.1 Criteria for the different TC expressions

In previous studies, three different expressions have been widely utilized as the expression of TC, which are different in (i) the way how TC is expressed with phenomenological coefficients and/or in (ii) the way how the heat current is defined. In the present thesis, with focusing on the binary systems, three TC expressions will be compared and then the differences among them will be clarified by using theoretic means and by the result of MD simulations. This procedure will suggest the most appropriate TC expression and evaluate the error in the other two TC expressions. Based on the results of comparison between them, discussion is made about the advantages and disadvantages of the three TC expressions and about the conditions where a significant error may occur.

As for the models of binary systems, Li_2O and TiO_2 are selected: TiO_2 is a typical ionic material where the atomic mobility is low below the melting point, while Li_2O is known as a superionic conductor where Li diffuses like in a liquid even in the solid phase [21] at some high temperatures. This selection was made because the atomic mobility is one of the main factors to determine differences among the three TC expressions, as will be shown in this thesis.

2.2.1 First criterion – number of terms in TC expression

On the difference in (i) the TC expression itself, some studies express TC only with L_{QQ} as [4], [5], [7], [8], [12], [15], [16], [22]

$$\kappa_1 = \frac{L_{QQ}}{T^2}, \tag{2.2}$$

while others involve another combination of PCs as [6], [13], [14], [17], [18], [23]

$$\kappa_2 = \frac{1}{T^2}\left(L_{QQ} - \frac{L_{Q1}L_{1Q}}{L_{11}} \right), \tag{2.3}$$

where L_{1Q} and L_{Q1} are PCs on the correlation between the heat current and the mass current. In the present study, we denote the former one as single-term expression, and the latter as double-terms expression. While the single-term expression is often utilized for solids, the double-terms expression is mostly employed for fluids like plasma [23] or liquids, [6], [13], [14], [18] albeit the application to solids [17], [18] also sparsely exist. As the double-terms expression considers the cross-coupling phenomenon of the heat current with the mass current, or with the charge current, the strength of such

cross effect would make distinct the double-terms expression from the single-term expression.

2.2.2 Second criterion – definition of the heat current

With respect to the difference in (ii) the definition of the heat current, which is calculated as the time derivative of atomic energy moment in MD, some studies subtract the partial specific enthalpy (PSE) from the atomic energy [4], [5], [7], [22], [24] while others do not [8], [12], [15], [16]. This difference introduces two distinct microscopic heat current expressions under the zero barycentric velocity condition as

$$\begin{aligned}\mathbf{j}_Q^*(t) &= \frac{d}{dt}\sum_{i=1}^{N}\mathbf{r}_i(t)e_i(t) \\ &= \sum_{i=1}^{N}\mathbf{v}_i(t)e_i(t) + \sum_{i=1}^{N}\left[\sum_{j=1,\neq i}^{N}\mathbf{F}_{ij}(t)\cdot\mathbf{v}_j(t)\right]\mathbf{r}_{ij}(t),\end{aligned} \tag{2.4}$$

for the PSE non-subtracted form [24], and

$$\mathbf{j}_Q(t) = \mathbf{j}_Q^*(t) - \sum_{k=1}^{2} \overline{h}_k \mathbf{j}_k(t),$$
$$\mathbf{j}_k(t) = \sum_{i=1}^{N_k} m_k \mathbf{v}_i^k(t), \tag{2.5}$$

for the PSE subtracted form, where N is the total number of atoms, $\mathbf{r}_i$ is the position vector ($\mathbf{r}_{ij} = \mathbf{r}_i - \mathbf{r}_j$), e_i is the total energy (kinetic + potential) of atom i, $\mathbf{F}_{ij}$ is the force acting on atom i due to atom j, m_k is the atomic mass, and $\overline{h}_k$ is the PSE of component k ($\overline{h}_k = h_k / m_k$, where h_k is the partial molar enthalpy). Note that an upper bar is used to denote a mass-specific quantity in the present paper. Differently from Refs. [18], [21] and [22], we define PSE as a mass-specific quantity because we use the mass current instead of the molar current for the description of the irreversible processes in the present study.

It should be noted that there has been an inconsistency on how $\mathbf{j}_A$ quantity is named in previous studies: some studies call it flux of A, while others current of A. In the present study, we define a PC as a volume-divided and do not define $\mathbf{j}_A$ as a volume-divided quantity. While the unit of a flux is usually [#/m^2·s], where # is the number of particles, the unit of a current is [#·m/s]. Thus it is more appropriate to call $\mathbf{j}_A$ as a current rather than a flux in the present paper. There has also been a great confusion in the way how $\mathbf{j}_Q^*$ and $\mathbf{j}_Q$ are named. $\mathbf{j}_Q^*$ and $\mathbf{j}_Q$ are respectively named as heat current

and reduced heat current in some studies, while energy current and heat current in other studies. Since the concept of heat is a flow of excess energy in general, the latter may be more apropos. However, regardless of the name, they should be thoroughly distinguished so as to allude their obvious difference in the result of TC calculation. For convenience of writing, I shall adopt the former nomenclature in this thesis, namely heat current for $\mathbf{j}_Q^*$ and reduced heat current for $\mathbf{j}_Q$. Throughout the present manuscript, an upper asterisk is used for expression of a non-reduced quantity in order to distinguish a non-reduced one and a reduced quantity.

Using these notations, TC expressions of Eqs. (2.2) and (2.3) with the PSE non-subtracted heat current are written as

$$\kappa_1^* = \frac{L_{Q^*Q^*}}{T^2}, \tag{2.6}$$

and

$$\kappa_2^* = \frac{1}{T^2}\left(L_{Q^*Q^*} - \frac{L_{Q^*1}L_{1Q^*}}{L_{11}} \right). \tag{2.7}$$

It has been shown that the double-terms expressions κ_2^* and κ_2 are equivalent to each other for binary systems under the condition of fixed center of mass [13]. This is consequence of the fact that these expressions are derived from identical entropy production, which will be explained in later section. Thus the double terms expressions liberate the choice of heat current in TC calculation, which was proven at least.

For a single component system, Hoheisel pointed out that the subtraction of PSE does not change the value of TC when the center of mass is fixed, [27] thus $\kappa_1^* = \kappa_1$. The condition of fixed center of mass makes the component mass current zero in a single-component system. For multi-component systems, however, remaining of PSE term in the heat current induces some differences in the resultant TC, namely $\kappa_1^* \neq \kappa_1$, because instantaneous values of the component mass currents in MD simulations are usually not zero even if the total center of mass is fixed.

To sum up, there are three essentially different versions of the TC expression in EMD with the GK relation for binary systems, namely κ_1^*, κ_1, and κ_2, as summarized in Table 2.1.

Table 2.1. Summary of different thermal conductivity expressions

Reference of classification		Types of heat current	
		Reduced heat current	Ordinary heat current
Number of terms	Single term	$\kappa_1 = \frac{L_{QQ}}{T^2}$	$\kappa_1^* = \frac{L_{Q^*Q^*}}{T^2}$
	Double terms	$\kappa_2 = \frac{1}{T^2}\left(L_{QQ} - \frac{L_{Q1}L_{1Q}}{L_{11}}\right)$	$\kappa_2^* = \frac{1}{T^2}\left(L_{Q^*Q^*} - \frac{L_{Q^*1}L_{1Q^*}}{L_{11}}\right)$

Chapter 3. Theoretical Backgrounds

3.1 Entropy production for the irreversible processes

In previous studies, the entropy production in the non-equilibrium thermodynamics has been used as the starting point to obtain a theoretical expression of TC [6],[12],[23],[24]. The entropy production is expressed with multiplication of a current quantity and a corresponding thermodynamic force. Under the assumption that there is no external electric and magnetic fields and no viscous friction [6], the entropy production is written as [29]

$$\sigma = \mathbf{J}_Q^* \cdot \nabla\left(\frac{1}{T}\right) - \sum_{k=1}^{2} \mathbf{J}_k \cdot \nabla\left(\frac{\bar{\mu}_k}{T}\right), \tag{3.1}$$

where σ is the entropy source strength per second, $\mathbf{J}_Q^*$ and $\mathbf{J}_k$ are the heat current and mass current, respectively. The subscript k denotes the component index. $\bar{\mu}_k$ is the specific electrochemical potential including the Coulomb interaction energy between constituent ions in MD simulations.

The Gibbs-Helmholtz equation [28] let us expand the gradient in the second term as

$$T\nabla\left(\frac{\bar{\mu}_k}{T}\right)=-\frac{\bar{h}_k}{T}\nabla T+\nabla_T\bar{\mu}_k. \tag{3.2}$$

The subscript T at the gradient operator means that the gradient is taken under the constant temperature condition. Consequently, we can rewrite the entropy production as

$$\sigma=-\frac{1}{T^2}\mathbf{J}_Q^*\nabla T+\sum_{k=1}^{2}\mathbf{J}_k\frac{\bar{h}_k}{T^2}\cdot\nabla T-\sum_{k=1}^{2}\mathbf{J}_k\frac{1}{T}\cdot\nabla_T\bar{\mu}_k \tag{3.3}$$

Note that the current quantities in Eq. (3.3) are macroscopic ones, not microscopic ones, in the viewpoint of the irreversible thermodynamics. Nevertheless, previous researches adopting the same approach starting from the entropy production suggest that applications of this theory to MD are widely conducted. For clarity, we use **J** for a macroscopic current and **j** for a microscopic current in this article. Note also that Eq. (3.3) is a typical expression of the entropy production for describing irreversible processes in previous studies regardless of NEMD [6], [30] and EMD [13] approach.

3.2 Trace of the origin of TC expressions

In this section, we trace several possible ways to obtain the TC expressions introduced in Table 2.1. However, the derivation processes presented here are neither theoretically immaculate, nor absolute ones. Rather, those derivations are suggesting one of the possibility that each of TC expressions would be obtained as result of the processes. Nonetheless, we believe that these derivation processes are informative in that they provide physical insights for the differences between TC expressions, which are otherwise too abstruse and abstractive to understand. Basically, the derivation procedure made here are organized as going from the entropy production, through phenomenological equations, to the final TC expression. Before beginning in earnest about the derivation procedure, however, it is worth to note beforehand about the significance of an important assumption, which is $\mathbf{J}_1 = 0$.

3.2.1 About the assumption of $\mathbf{J}_1 = 0$

As the assumption of $\mathbf{J}_1 = 0$ appears commonly in the derivation processes of every TC expressions introduced in this thesis and also in previous studies, it is important to understand why this assumption is made for the TC. This assumption originates from the experimental method, say it is the laser-flash method as an example. In the laser-flash method, firstly one

side of sample is fired by the laser flash. Due to the flashing laser, the temperature gradient within the sample is established. For this instantaneous moment, there should also be the gradient of chemical potential gradient established at the same time due to the different temperature of both sides within the sample. Here, the sample has two competing thermodynamic forces: temperature gradient and chemical potential gradient. They compete for atoms to move toward different directions of sample, respectively: If the temperature gradient is settled from left to right, the atom tends to move from right to left, but because the chemical potential gradient is settled from right to left, this forces an atom to move left to right. Therefore, after a while the sample reaches to the steady-state where there is no net movement of atoms in a sample, where $\mathbf{J}_1 = 0$. This would be an acceptable assumption without such complex consideration, because normally one do not consider the TC when there is a net movement of atoms in a system.

3.2.2 Double terms expressions: κ_2 and κ_2^*

Combining the 1st and the 2nd terms in Eq. (3.3) gives

$$\begin{aligned}\sigma &= -\frac{1}{T^2}\left(\mathbf{J}_Q^* - \sum_{k=1}^{2}\bar{h}_k\mathbf{J}_k\right)\nabla T - \sum_{k=1}^{2}\mathbf{J}_k\frac{1}{T}\nabla_T\bar{\mu}_k \\ &= -\frac{1}{T^2}\mathbf{J}_Q\nabla T - \sum_{k=1}^{2}\mathbf{J}_k\frac{1}{T}\nabla_T\bar{\mu}_k,\end{aligned} \tag{3.4}$$

where the reduced heat current is introduced as

$$\mathbf{J}_Q = \mathbf{J}_Q^* - \sum_{k=1}^{2} \overline{h}_k \mathbf{J}_k . \tag{3.5}$$

If we use the zero barycentric velocity condition, $\mathbf{J}_1 = -\mathbf{J}_2$ holds, and then Eq. (3.5) can be rewritten as

$$\begin{aligned} \sigma &= -\frac{1}{T^2}\mathbf{J}_Q \nabla T - \mathbf{J}_1 \frac{1}{T} \nabla_T \overline{\mu}_1 + \mathbf{J}_1 \frac{1}{T} \nabla_T \overline{\mu}_2 \\ &= -\frac{1}{T^2}\mathbf{J}_Q \nabla T - \frac{1}{T}\mathbf{J}_1 \left(\nabla_T \overline{\mu}_1 - \nabla_T \overline{\mu}_2 \right). \end{aligned} \tag{3.6}$$

Defining a new state variable $\overline{\mu}_m = \overline{\mu}_1 - \overline{\mu}_2$, we finally arrive at an entropy production comprised of the reduced heat current and the mass current,

$$\sigma = \mathbf{J}_Q \underbrace{\left(-\frac{\nabla T}{T^2} \right)}_{\mathbf{X}_Q} + \mathbf{J}_1 \underbrace{\left(-\frac{\nabla \overline{\mu}_m}{T} \right)}_{\mathbf{X}_1}. \tag{3.7}$$

where $\mathbf{X}_1$ and $\mathbf{X}_Q$ are the direct thermodynamic forces for the heat current and mass current, respectively. At the same time, both $\mathbf{X}_1$ and $\mathbf{X}_Q$ can act as a cross driving force, conjugated by cross phenomenological coefficient, as shown in the following phenomenological equations corresponding to the entropy production of Eq. (3.7)

$$\mathbf{J}_Q = -L_{QQ}\frac{\nabla T}{T^2} - L_{Q1}\frac{\nabla \bar{\mu}_m}{T}, \tag{3.8}$$

$$\mathbf{J}_1 = -L_{1Q}\frac{\nabla T}{T^2} - L_{11}\frac{\nabla \bar{\mu}_m}{T}. \tag{3.9}$$

Here, as done in previous studies [14], [31] we apply $\mathbf{J}_1 = 0$ assumption. Note that the $\mathbf{J}_1 = 0$ assumption is applied at the level of phenomenological equations. Subsequently, we substitute $\nabla \mu_m$ in Eq. (3.8) with that in Eq. (3.9), yielding

$$\mathbf{J}_Q = -\frac{1}{T^2}\left(L_{QQ} - \frac{L_{Q1}L_{1Q}}{L_{11}} \right)\nabla T, \tag{3.10}$$

$$\kappa_2 = \frac{1}{T^2}\left(L_{QQ} - \frac{L_{Q1}L_{1Q}}{L_{11}} \right). \tag{3.11}$$

Although L_{IQ} and L_{QI} are equivalent with each other according to the Onsager's reciprocal relation [32], we do not merge them here for the purpose of later discussions.

To achieve κ_2^*, Eq. (3.3) is arranged using the $\mathbf{J}_1 = -\mathbf{J}_2$ condition again as

$$\begin{aligned}\sigma &= \mathbf{J}_Q^*\left(-\frac{1}{T^2}\nabla T\right) + \mathbf{J}_1\frac{1}{T^2}\cdot\nabla T\left(\bar{h}_1 - \bar{h}_2\right) - \mathbf{J}_1\frac{1}{T}\left(\nabla_T(\bar{\mu}_1 - \bar{\mu}_2)\right) \\ &= \mathbf{J}_Q^*\underbrace{\left(-\frac{1}{T^2}\nabla T\right)}_{\mathbf{x}_Q^*} + \mathbf{J}_1\underbrace{\left\{\frac{1}{T^2}\left(\bar{h}_1 - \bar{h}_2\right)\nabla T - \frac{1}{T}\nabla_T\bar{\mu}_m\right\}}_{\mathbf{x}_1^*}.\end{aligned} \tag{3.12}$$

Then the phenomenological equation is described as

$$\mathbf{J}_Q^* = -L_{Q^*Q^*}\frac{\nabla T}{T^2} + L_{Q^*1}\left(\frac{1}{T^2}\left(\bar{h}_1 - \bar{h}_2\right)\nabla T - \frac{1}{T}\nabla_T\bar{\mu}_m\right), \tag{3.13}$$

$$\mathbf{J}_1 = -L_{1Q^*}\frac{\nabla T}{T^2} + L_{11}\left(\frac{1}{T^2}\left(\bar{h}_1 - \bar{h}_2\right)\nabla T - \frac{1}{T}\nabla_T\bar{\mu}_m\right). \tag{3.14}$$

In a similar procedure to that for κ_2, applying $\mathbf{J}_1 = 0$ assumption the κ_2^* is obtained as

$$\mathbf{J}_{Q}^{*}=-\frac{1}{T^{2}}\left(L_{Q^{*}Q^{*}}-\frac{L_{Q^{*}1}L_{1Q^{*}}}{L_{11}}\right)\nabla T, \tag{3.15}$$

$$\kappa_{2}^{*}=\frac{1}{T^{2}}\left(L_{Q^{*}Q^{*}}-\frac{L_{Q^{*}1}L_{1Q^{*}}}{L_{11}}\right). \tag{3.16}$$

For the derivation of κ_2 and κ_2^*, there is no difference in the entropy production essentially, between Eqs. (3.4) and (3.12). This leads to a natural consequence that these double terms TC expressions are equivalent to each other, as shown in Ref. 12. Note that in Ref. 12, instead of using the mass current, the double terms TC expression was obtained by using the charge current which was defined as $\mathbf{J}_Z=\sum_k \overline{q}_k\mathbf{J}_k$, where $\overline{q}_k$ is the specific atomic charge. This charge current expression differs with the mass current defined here only by a scaling constant, which made the double terms TC expression in Ref. 12 be equivalent to Eqs. (3.11) and (3.16).

3.2.3 Single terms expressions: κ_1 and κ_1^*

If we neglect the third term in Eq. (3.3), the entropy production becomes solely composed of the reduced heat current as

$$\sigma = -\frac{1}{T^2}\mathbf{J}_Q^*\nabla T + \sum_{k=1}^{2}\mathbf{J}_k\frac{\bar{h}_k}{T^2}\cdot\nabla T$$
$$= \mathbf{J}_Q\underbrace{\left(-\frac{\nabla T}{T^2}\right)}_{\mathbf{x}_Q}. \tag{3.17}$$

The phenomenological equation and TC expression corresponding to this entropy production are respectively obtained as

$$\mathbf{J}_Q = -L_{QQ}\frac{\nabla T}{T^2}, \tag{3.18}$$

$$\kappa_1 = \frac{L_{QQ}}{T^2}. \tag{3.19}$$

It can be noticed that κ_1 is just the first term of κ_2, where the L_{QQ} represents the strength of the autocorrelation of the reduced heat current.

This κ_1 expression can be alternatively obtained by the simple neglect of the second term in Eq. (3.8), where the manipulation is made at the level of the phenomenological equations. By this way, even though we do not go up to the entropy production, we can obtain the equivalent κ_1 expression. As we leave the entropy production of Eq. (3.3) intact, we are still dealing with a situation where both driving forces (∇T and $\nabla\bar{\mu}_m$) exists. Therefore,

this derivation corresponds to consider L_{1Q} as zero in Eq. (3.8), which conjugates the phenomenological current and its indirect driving force.

To obtain κ_1^*, we further neglect the second term in Eq. (3.3), which gives the simplest entropy production as

$$\sigma = \mathbf{J}_Q^* \underbrace{\left(-\frac{\nabla T}{T^2} \right)}_{\mathbf{x}_Q}. \tag{3.20}$$

In a similar procedure to that for κ_1, we can obtain

$$\mathbf{J}_Q^* = -L_{Q^*Q^*} \frac{\nabla T}{T^2}, \tag{3.21}$$

$$\kappa_1^* = \frac{L_{Q^*Q^*}}{T^2}. \tag{3.22}$$

Among several number of cases, it is possible to interpret the neglect of second and third term in Eq. (3.3) for κ_1^* derivation, as the assumption of $\mathbf{J}_1 = 0$ is made in the entropy production. If the component mass current is zero in reality, this derivation process of κ_1^* would not degrade the

accuracy of Eq. (3.3). However, as $\mathbf{J}_1 = 0$ is a hardly achieved for multi component systems in MD simulations. Especially for certain conditions such as high temperature or disordered phase where atoms are mobile in MD simulations, the resultant κ_1^* has a possibility to show an abnormal value.

The scrutiny in the current section suggests how each TC expression can be derived. At the same time, it is clarified how the reduced heat current appears. The origin of differences among the three TC expressions can be traced back to the derivation processes introduced so far. The commonly tried approaches for the derivations of every TC expressions have started from the entropy production. By the adequate manipulations, we get different entropy production, which denotes the different degree of details in the description of irreversible phenomena: the more terms exist in the entropy production, we believe the more accurate description of irreversible phenomena is being made. The differences in the entropy production for the three TC expressions are described by under brackets in Eq. (3.3). From the discussions made so far, it is reasonable to consider that κ_2 as the most accurate TC expression, because it accompanies the least amount of assumptions for its derivation compared to the remaining two TC expressions. Therefore, we regard κ_2 as the reference TC value for the evaluation of error in the other two TC expressions.

3.3 Analysis of the difference between TC expressions

The PCs appeared in the TC expressions are written as [6], [13]

$$
\begin{aligned}
L_{Q^*Q^*} &= \frac{1}{3k_B \mathrm{V}} \int_0^\infty \left\langle \mathbf{j}_Q^*(0) \cdot \mathbf{j}_Q^*(t) \right\rangle dt, \\
L_{QQ} &= \frac{1}{3k_B \mathrm{V}} \int_0^\infty \left\langle \mathbf{j}_Q(0) \cdot \mathbf{j}_Q(t) \right\rangle dt, \\
L_{1Q} &= \frac{1}{3k_B \mathrm{V}} \int_0^\infty \left\langle \mathbf{j}_Q(0) \cdot \mathbf{j}_1(t) \right\rangle dt, \\
L_{11} &= \frac{1}{3k_B \mathrm{V}} \int_0^\infty \left\langle \mathbf{j}_1(0) \cdot \mathbf{j}_1(t) \right\rangle dt.
\end{aligned}
\tag{3.23}
$$

The definitions of $\mathbf{j}_Q$, $\mathbf{j}_Q^*$ and $\mathbf{j}_1$ are given in Eqs. (2.4). Note that here $\mathbf{j}_Q$, $\mathbf{j}_Q^*$ and $\mathbf{j}_1$ are microscopic quantities, not macroscopic ones.

In this section, the differences among the three TC expression are described in connection with the properties of material. We will first introduce the expression of PSE, the heat of transport and the Maxwell-Stefan (MS) diffusion coefficient, which will be used to describe the differences among the three TCs.

3.3.1 Partial specific enthalpy

Under the zero barycentric velocity condition, the reduced heat current is expressed as

$$\begin{aligned}\mathbf{j}_Q(t) &= \mathbf{j}_Q^*(t) - \overline{h}_1\mathbf{j}_1(t) - \overline{h}_2\mathbf{j}_2(t) \\ &= \mathbf{j}_Q^*(t) - (\overline{h}_1 - \overline{h}_2)\mathbf{j}_1(t) \\ &= \mathbf{j}_Q^*(t) - \Delta\overline{h}\cdot\mathbf{j}_1(t).\end{aligned} \tag{3.24}$$

Unless the component mass current is zero, $\Delta\overline{h}$ term alters the value of the reduced heat current and thus may affect TC. To calculate the reduced heat current, the exact value of PSE for each component is necessary. Basically, PSE is determined by dividing partial molar enthalpy by the atomic mass. However, the calculation of partial molar enthalpy in MD simulation is known as a difficult task due to the strong thermodynamic constraints: constant temperature, pressure, and number of moles of other components [13]. We utilize a successful microscopic expression [22], [33] for PSE, which is given as

$$\overline{h}_k = \overline{u}_k + \overline{p_k V}, \tag{3.25}$$

$$\overline{p_k V} = \frac{1}{3m_k N_k}\left\langle \sum_{\alpha=1}^{3}\sum_{i=1}^{N_k} S_{\alpha\alpha}^{i,k}\cdot V \right\rangle, \tag{3.26}$$

$$S_{\alpha\alpha}^{i,k}\cdot V = m_k v_{i,\alpha}^k v_{i,\alpha}^k + \frac{1}{2}\left(\sum_{j=1,\neq i}^{N} F_{ij,\alpha}\cdot r_{ij,\alpha} \right), \tag{3.27}$$

where p_k denotes the partial pressure term in the definition of enthalpy, $\overline{u}_k$ is the averaged component atomic energy including kinetic and potential contributions, and $\mathbf{S}_{\alpha\beta}^{i,k}$ is the atomic stress tensor. The partial pressures are related to the total system pressure p as

$$p = p_1 N_1 + p_2 N_2 . \tag{3.28}$$

In a MD simulation, the $\overline{u}_k$ has a non-zero absolute value which originates from the potential model utilized. However, the absolute value of $\overline{u}_k$ itself lacks a physical significance due to, for example, the vague idea about in which condition the absolute value of $\overline{u}_k$ becomes zero. In other words, we have uncertain definition of state where the $\overline{u}_k$ is zero. Utilization of $\overline{u}_k$ instead of $\overline{h}_k$ as a representative average atomic energy alleviates such problem regarding the set of reference energy state. Thus the subtraction of this PSE from the non-reduced heat current as in Eq. (3.24) guarantees that we can treat the excess energy transport phenomenon in a system, which is reasonably consistent with the definition of heat.

3.3.2 Heat of transport

According to Refs. [31] and [32], the heat of transport $\overline{Q}_k^*$ and the reduced heat of transport $\overline{Q}_k$ are respectively defined as

$$\mathbf{J}_Q^* = \sum_{k=1}^{n-1} \overline{Q}_k^* \mathbf{J}_k, \ (\nabla T = 0) \tag{3.29}$$

$$\mathbf{J}_Q = \sum_{k=1}^{n-1} \overline{Q}_k \mathbf{J}_k, \ (\nabla T = 0) \tag{3.30}$$

The reduced heat of transport is expressed by PCs as

$$\overline{Q}_k = \sum_{i=1}^{n-1} \frac{L_{qi}}{L_{ki}}, \ (k = 1, \ 2, \ ..., \ n-1), \tag{3.31}$$

where n is the number of components (e.g. 2 in Li_2O) in the system. In a binary system, there is only one independent reduced heat of transport $\overline{Q}_1$, which is equal to L_{q1}/L_{11}. From its definition, the reduced heat of transport represents the amount of excess energy transferred by the mass current [36], where an excess energy is calculated by subtracting $\overline{h}_k$ from an

instantaneous atomic energy at a certain timing. It is easy to show the relation between the heat of transport and the reduced heat of transport as

$$\bar{Q}_1^* = \Delta\bar{h} + \bar{Q}_1 \tag{3.32}$$

3.3.3 Maxwell-Stefan diffusion coefficient

The MS diffusion coefficient relates the mass current with its correct driving force, namely the chemical potential gradient, and is defined as [26]

$$\sum_{j\neq i=1}^{n} \frac{x_j(\mathbf{u}_i - \mathbf{u}_j)}{Đ_{ij}} = -\frac{\nabla\mu_i}{k_B T}, \tag{3.33}$$

where x_j is the mole fraction, $\mathbf{u}_j$ is the center of mass velocity of component j, and $Đ_{ij}$ is the MS diffusion coefficient which couples the mass current of component i and the chemical potential gradient of component j. For the calculation of MS diffusion coefficient by the GK relation, we follow the approach of Guevara-Carrion et al.,[26] which gives the related PC as

$$Ł_{kl} = \frac{1}{3N}\int_0^{\infty}\left\langle \sum_{i=1}^{N_k} v_i^k(0)\cdot\sum_{j=1}^{N_l} v_j^l(t)\right\rangle dt. \tag{3.34}$$

Note that, as molar currents are used in Ref. 26 instead of mass currents, there is a difference in the definitions between $Ł_{kl}$ and L_{kl}, which is expressed as

$$Ł_{kl} = \frac{k_B V}{N m_k m_l} L_{kl}. \tag{3.35}$$

The MS diffusion coefficient for a binary system is given as [26], [37]

$$Đ_{12} = \frac{x_2}{x_1} Ł_{11} + \frac{x_1}{x_2} Ł_{22} - Ł_{12} - Ł_{21}. \tag{3.36}$$

Using the zero barycentric velocity condition, we have

$$\sum_{i=1}^{N_1} v_i^1(t) = -\frac{m_2}{m_1}\sum_{j=1}^{N_2} v_j^2(t). \tag{3.37}$$

Consequently, the four PCs in Eq. (3.36) are reduced into one PC as

$$\begin{aligned} Đ_{12} &= \left(\frac{x_2}{x_1} + \frac{x_1}{x_2}\left(\frac{m_1}{m_2}\right)^2 + 2\left(\frac{m_1}{m_2}\right) \right) Ł_{11} \\ &= M \cdot Ł_{11}, \end{aligned} \tag{3.38}$$

where M is a material-specific constant. The value of M is 1.76 for Li_2O and 12.5 for TiO_2.

3.3.4 Difference between TC expressions

In MD simulations, a continuous-time integration from 0 to $+\infty$ is substituted with a discrete-time summation up to a finite time length, which is called as the correlation length. Specifically, the GK relation of Eq. (2.1) is implemented in MD as

$$L_{AB} = \frac{1}{3k_B V}\left(\frac{1}{N_S+1}\frac{1}{N_T+1}\sum_{i=0}^{N_S}\sum_{j=0}^{N_T} \mathbf{j}_A(i\Delta t)\,\mathbf{j}_B((i+j)\Delta t) \right), \tag{3.39}$$

where N_T denotes the correlation length. As we only integrate the GK relation up to the correlation length, we can have multiple number of

correlation which starts at the different instant during the whole MD simulation. This fact enable us to have statistically more accurate correlation function, which is expressed as the average of the number of sampling, N_S in Eq. (3.39). With this discretized expression of GK relation, analysis on the differences among the three TC expressions becomes more explicit.

3.3.4.1 Difference between κ_1 and κ_2

From the comparison between Eqs. (3.11) and (3.19), the difference between κ_1 and κ_2 is just the 2nd term of κ_2. By expressing this second term in terms of MS diffusion coefficient using Eqs. (3.35) and (3.38), the difference is written as

$$\kappa_1 - \kappa_2 = \bar{Q}_1^{\,2} \cdot \frac{Nm_1^2}{Mk_B VT^2} D_{12}. \tag{3.40}$$

In Section 3.2.2, from the view point of the derivation of κ_1 from the phenomenological equations, the cross-phenomenological coefficient L_{1Q} is neglected. Because of the manipulation, the cross-correlation between the heat current and the mass current disappears. Thus we call this difference as "Cross effect". Note that the Cross effect is always a positive value.

3.3.4.2 Difference Between κ_1^* *and* κ_1

By using Eq. (3.39), the PC of reduced heat current is written as

$$
\begin{aligned}
L_{Q^*Q^*} &= \frac{1}{3k_BV}\left(\frac{1}{N_S+1}\frac{1}{N_T+1}\sum_{i=0}^{N_S}\sum_{j=0}^{N_T}\mathbf{j}_Q^*(i\Delta t)\,\mathbf{j}_Q^*((i+j)\Delta t)\right)\\
&= \frac{1}{3k_BV}\frac{1}{N_S+1}\frac{1}{N_T+1}\sum_{i=0}^{N_S}\sum_{j=0}^{N_T}\left(\mathbf{j}_Q(i\Delta t)+\Delta\bar{h}\cdot\mathbf{j}_1(i\Delta t)\right)\left(\mathbf{j}_Q((i+j)\Delta t)+\Delta\bar{h}\cdot\mathbf{j}_1((i+j)\Delta t)\right)\\
&= L_{QQ}+\Delta\bar{h}\cdot L_{1Q}+\Delta\bar{h}\cdot L_{Q1}+(\Delta\bar{h})^2L_{11}\\
&= L_{QQ}+\left(2\Delta\bar{h}\cdot\bar{Q}+(\Delta\bar{h})^2\right)L_{11}\\
&= L_{QQ}+\left(2\Delta\bar{h}\cdot\bar{Q}+(\Delta\bar{h})^2\right)\frac{Nm_1^2}{k_BV}Ł_{11}.
\end{aligned}
\tag{3.41}
$$

The third line in Eq. (3.41) applies the Onsager's reciprocal relation [32]. Dividing both sides by temperature square, the difference of TC is expressed in terms of MS diffusion coefficient as

$$
\kappa_1^*-\kappa_1=\left(\underbrace{2\Delta\bar{h}\cdot\bar{Q}_1}_{\text{1st term}}+\underbrace{(\Delta\bar{h})^2}_{\text{2nd term}}\right)\frac{Nm_1^2}{Mk_BVT^2}Đ_{12}. \tag{3.42}
$$

By Eqs. (3.40) and (3.42), it can be seen that both TC differences hold similar forms of "(energy)^2×(diffusion coefficient)×(constants)". Strictly speaking, in the "constants" group there is volume and temperature term, both of which are apparently temperature dependent. As the temperature dependency of these volume and temperature is rather straight forward than the other terms, we still note the Nm_1^2 / Mk_BVT^2 as "constants" and stick on the investigation of the others: "energy" and "diffusion coefficient".

In the 2nd term of Eq. (3.42), the role of $\bar{Q}_1$ in Eq. (3.40) is replaced with $\Delta\bar{h}$. Following this, we note the 2nd term of Eq. (3.42) as "PSE effect", while we note the 1st term as "PSE-Cross effect", because it is proportional to both $\bar{Q}_1$ and $\Delta\bar{h}$. The PSE-Cross effect can be either positive or negative, while the 2nd term (PSE effect) is always positive. From their roles in Eqs. (3.40) and (3.42), we can consider $\bar{Q}_1$ and $\Delta\bar{h}$ as they are the characteristic energies of a material that determine the sizes of the contribution of the Cross effect, the PSE-Cross effect and the PSE effect, to the TC value. Figure. 1 summarizes the differences between TC expressions investigated so far.

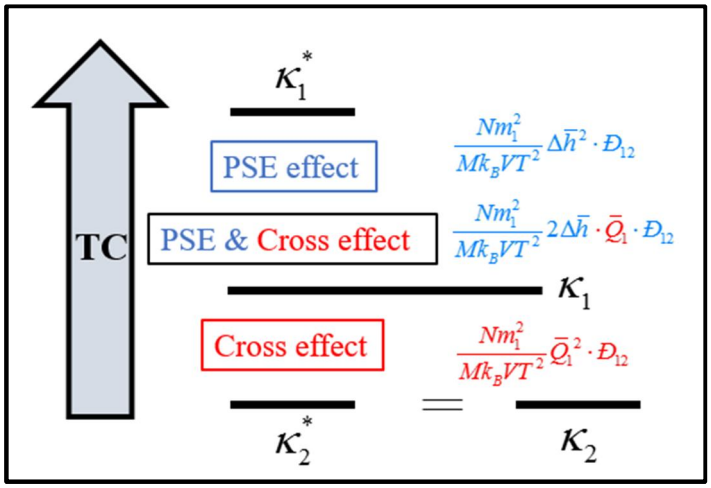

Figure. 3.1 Schematic diagram summarizing the difference between TC expressions.

3.3.4.3 Interpretation of the physical meaning of the difference between TC expressions

Concededly, $\mathbf{j}_Q^*$ of Eq. (2.4) is the most basic and fundamental expression which denotes the energy transport in a model system of MD simulation. As we use empirically fitted potential model for the energy and force calculation in MD, $\mathbf{j}_Q^*$ contains certain amount of energy of which its absolute value is physically groundless. The TC expression κ_1^* utilizes only the autocorrelation of this $\mathbf{j}_Q^*$. Therefore, we can consider κ_1^* as it represents the seemingly entire energy transport, where some portion of κ_1^* might not be suitable to the pure thermal conduction phenomenon.

Starting from this idea, we can assign the physical meaning of Eq. (3.40), as it is the contribution of energy transport via mass current driven by the chemical potential gradient. This contribution should be properly subtracted from the entire energy transport to accurately obtain the TC. And for the difference between κ_1 and κ_2, Eq. (3.40) can be interpreted as it is the contribution of energy transported by thermally driven mass current to TC.

Firstly, we visit the difference between κ_1 and κ_2. In the derivation of κ_1 from the level of the phenomenological equations, it is noticed that the assumption of $L_{1Q} = 0$ in Eq. (3.8) was involved. As the Onsager's reciprocal relation [32] holds for our formulations, we have $L_{Q1} = 0$ simultaneously in

Eq. (3.9), which suggests that we neglect contribution of temperature gradient to the mass current. In other words, the existence of this "thermally driven (indirectly driven) mass current" is neglected by using κ_1. However, there exists a possibility for this thermally driven mass current to possess the extra energy than the exact amount of activation energy for particles to diffuse, even though it might be a negligible amount in practice. Thus we lost information of energy transported by the thermally driven mass current by using κ_1 instead of κ_2. Here, the degree of the contribution of thermally driven mass current to TC is characterized by the square of the reduced heat of transport, $\bar{Q}_1$.

Secondly, for the difference between κ_1^* and κ_1, we have seen that κ_1^* can be obtained by the assumption of $\mathbf{J}_k = 0$. This component mass current can be driven by both the chemical potential gradient (direct) and the temperature gradient (indirect) driving forces. Note that we already quantified the contribution of thermally driven mass current to TC from the difference between κ_1 and κ_2. Therefore, the remaining contribution of $\mathbf{J}_k = 0$ to TC belongs to the effect of chemical potentially driven mass current.

Chapter 4. MD simulation

4.1 Details of calculation settings

4.1.1 Potential model and Model system

We performed MD simulations using LAMMPS [38] (Large-scale Atomic/Molecular Massively Parallel Simulator). Buckingham potential models parameterized by Vijayakumar *et al.* [39] and by Matsui *et al.* [40] were used for Li_2O and TiO_2, respectively. The coulombic term was evaluated by using the Ewald summation method [41]. The potential model for TiO_2 has been widely used and verified [42], [43] while that for Li_2O has not. This is because the model parameters for Li-Li and Li-O interactions in the potential model of Vijayakumar *et al.* [39] were constructed for Li_2TiO_3, where those for Ti-Ti, Ti-O, and O-O interaction are described with the potential model of Matsui *et al*. [44]. There exists other potential models for Li_2O whose applicability at high temperatures were verified [45], [46]. However, we used the present potential model because the main focus of the present study is to investigate the difference in the three TC expressions, not to accurately obtain a TC comparable with experiments, and we plan to study the validity of the three TC expressions in a ternary system in future by taking Li_2TiO_3 as an example.

To avoid the overlapping of the short-range pairwise interaction, the dimension of the supercell is usually set to supersede the twice of the cutoff radius (10 Å) of the potential model. Thereby we used 6×6×6 supercell for the anti-fluorite Li_2O crystal (2592 atoms), and 6×6×9 supercell for the rutile TiO_2 crystal (1944 atoms).

4.1.2 Equilibration and production run of MD simulation

For each system, the lattice constant was first determined by a 200 ps simulation of NPT ensemble. The target pressure was set to 0 atm, which is practically the same with 1 atm in simulations of condensed phases. The temperature was changed in two different manners: increasing and decreasing sequences, namely upward and downward sets, respectively. The upward set started with a perfect crystal, while the downward set with a liquid structure. Thus, the system is preferably equilibrated to be an ordered phase (crystal) in the upward set and to be a disordered phase (liquid or amorphous) in the downward set. In the present study, we evaluated TC values also in non-equilibrium phases such as super-cooled liquid and amorphous phases if such phases are stable enough for the calculation of material properties.

With the determined lattice constants at a target temperature, a supercell of the crystal was created. Subsequently, in the upward set, another 200 ps

simulation of NVT ensemble was conducted to relax the atomic position in the supercell at the target temperature. In the downward set, the supercell was firstly heated at 3000~5000 K for 50 ps with NVT ensemble to fully melt the system, and then was thermally equilibrated for 200 ps at the target temperature. After these equilibration runs, a 3~9 ns simulation was performed to extract the correlation functions of currents. We confirmed that the pressure of each system was fluctuating with centering at 0 atm during the production run. The timestep was set to be 1 fs in all simulations.

The correlation functions were sampled with 5 fs interval over 20 ~ 50 ps period depending on the TC value. In general, for a bigger TC value, a longer correlation length is needed to achieve a certain statistical accuracy because the phonon lifetime is longer. For each condition, we took an average of 9~12 independent simulations that had started with different initial atomic velocities in order to achieve better statistics of correlation functions.

4.2 Diffusion coefficient calculation

As shown in Eqs. (3.40) and (3.42), the diffusion coefficients are important parameters to determine differences among the three. We calculated self-diffusion coefficients using the Einstein relation of the mean-squared displacement (MSD), which is described as

$$D_1 = \lim_{t\to\infty} \frac{1}{6t} \left\langle \left| \mathbf{r}_i^1(t) - \mathbf{r}_i^1(0) \right|^2 \right\rangle, \tag{4.1}$$

where t is the time and **r** is the atomic position vector. The superscript and subscript of **r** denote an index of element and an index of atom of the specified element, respectively.

4.2.1 Set up of MSD limit

Since the position of an atom changes not only by displacement but also by thermal vibration, if the displacement length is comparable with the amplitude of the thermal vibration in an MD simulation, Eq. (4.1) cannot give reasonable values. We consider that the smallest diffusion distance needed for reasonable calculation of D_1 with Eq. (47) is around 2 Å, as the amplitude of thermal vibration is usually around 1 Å at high temperatures.

Under this criteria, the lowest diffusion coefficient that can be reasonably determined in the present simulation of 9 ns is 0.67 Å^2 / 9 ns $\approx$ 7.4×10^{-9} cm^2/s, which is hereafter called “MSD limit”.

4.2.2 Set up of GK limit

Additionally, since the GK relation can determine diffusion-related PCs (such as L_{11}, L_{1Q}, and L_{11}) only if a substantive diffusion event occurs [22], it is possible to set a lower limit of temperature above which the diffusion-related PCs are reasonably determined through the GK relation. We note this as the “GK limit”. This lower bound of temperature is concerned with the MS diffusion coefficient, the heat of transport and TC.

From this, one may wonder about the possibility or suitability of TC calculation at the temperatures lower than the GK limit. To say the result in advance, even though the properties related diffusion-related PCs such as MS diffusion coefficients are not accurately determined, it is possible to suggest a reasonable TC value at lower temperatures than the GK limit. This is because the error term suggested as Eq. (3.40) and (3.42) are negligible due to the low value of diffusion coefficient. Meanwhile, as the L_{QQ}, which is the most important PC, is independent of GK limit, any of TC expressions can give a reasonable TC result.

The determination of the GK limit is basically based on the value of MSD limit, as the occurrence of diffusion event is easily captured by the

MSD limit. In the current simulation results, both limits are set based on the component of index 1 (Li for Li_2O, and Ti for TiO_2) for each system. To be exact, it would be better to choose the index of fast diffusing component for the set up of these limitations. However for TiO_2 in current study, there is no substantial difference between the self-diffusion coefficient of Ti and O, making no big different in the choice of index. As a result, the GK limit temperature is set to be around 480 K for Li_2O and 1200 K for TiO_2, respectively.

By definition, the MS diffusion coefficient is obtained with Eq. (3.38) using several PCs calculated by the GK relation. For the purpose of further discussion, we introduce one simple approximation for the MS diffusion coefficient which can be obtained with self-diffusion coefficients, namely the the Darken's relation [47] as follows:

$$Đ_{12}^{approx.} = x_2 D_1 + x_1 D_2 . \tag{4.2}$$

The difference between $Đ_{12}^{approx.}$ and $Đ_{12}$ is described with a thermodynamic factor as $Đ_{12} = \Gamma \cdot Đ_{12}^{approx.}$ [26], which is defined as

$$\Gamma = \frac{d \ln a_1}{d \ln x_1} = \frac{d \ln a_2}{d \ln x_2}, \tag{4.3}$$

where a_k is the activity of component k. In Section 5.1, the accuracy of $Đ_{12}^{approx.}$ will be investigated in comparison with $Đ_{12}$ directly determined by the GK relation, and the usefulness of $Đ_{12}^{approx.}$ will be presented in later section.

Chapter 5. Results

5.1 Phases observed in the MD simulation

Since the simulations were performed over a wide temperature range including temperatures above the melting point, several phases were observed in the MD simulations. First of all, we identify phases appeared in the MD simulations by analyzing changes in the supercell volume and diffusion coefficients.

5.1.1 Li_2O Model system

Figures. 5.1 show the temperature dependences of the supercell volumes of Li_2O and TiO_2 in the upward and downward sets. In the Li_2O upward set, a phase transition is indicated by a sudden increase of the volume between 1000 K and 1200 K. Hence the melting point of Li_2O with the present potential model is around 1100 K, which we also determined by checking the stability of solid-liquid interface in a simulation system composed of a crystalline region and a liquid region, namely the simulation of coexisting phases [48]. Note that this melting temperature is far below the experimental melting point (1711 K [49]).

There are large differences in Fig. 5.1(a) between results of the upward and downward sets at 800 ~ 1000 K. This difference is caused by appearance of a metastable supercooled liquid phase in the downward set at 800 ~ 1000 K. In the upward set, the systems were crystalline solid in this temperature range.

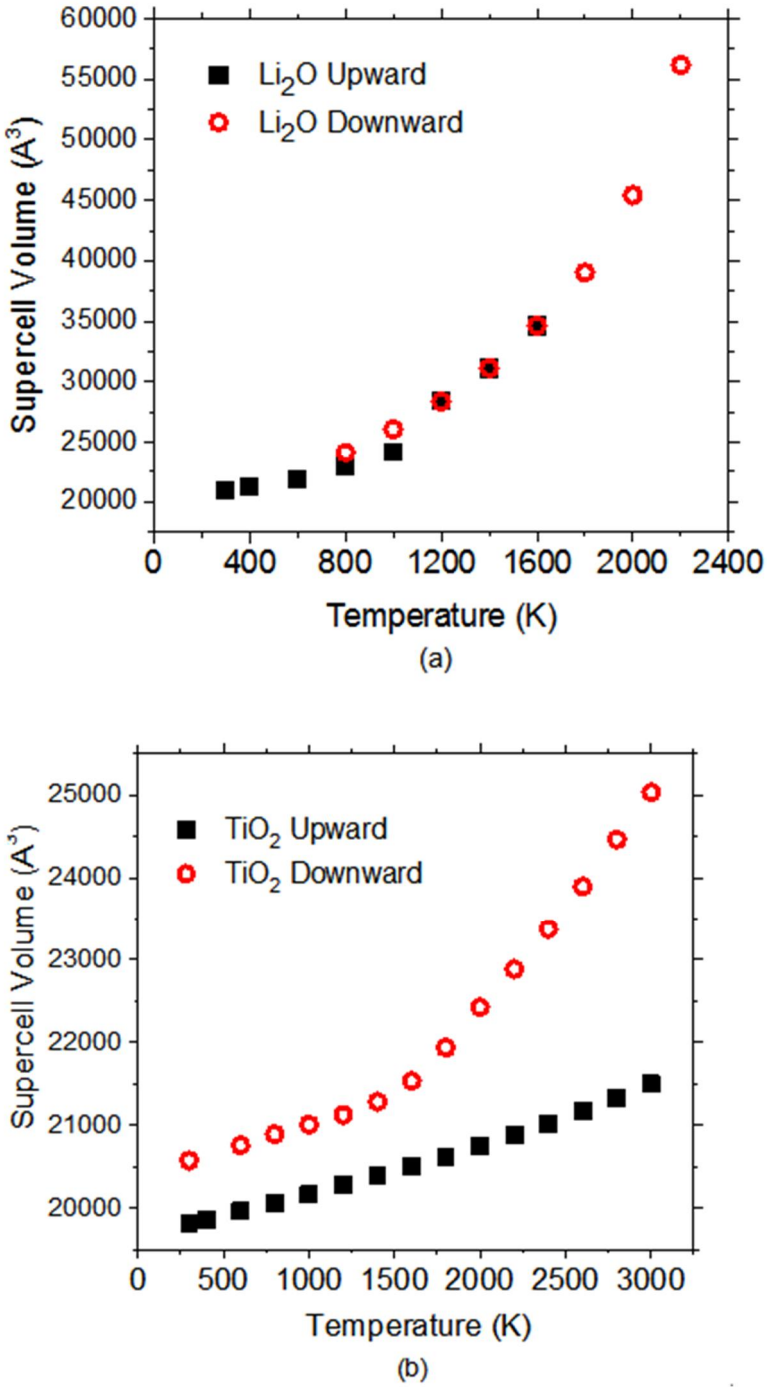

Figure. 5.1 Supercell volume change of (a) Li_2O and (b) TiO_2 system.

Figures. 5.2 show the result of diffusion coefficients of Li_2O and TiO_2 model system. In Fig. 5.2(a) for Li_2O, large value of self-diffusion coefficients are observed at 800~1000 K in the downward set for both Li and O, confirming the appearance of super-cooled liquid state. Note that the typical self-diffusion coefficient of a liquid state is around $D^{self} \approx 10^{-6}$ cm^2/s.

In the Li_2O downward set, re-crystallization quickly occurred for 600 K and 800 K, so that an amorphous phase did not appear in the simulation of Li_2O. Since the re-crystallization usually resulted in a crystal with various defects, not in a perfect crystal, the system was not stable enough to calculate material properties. For example, the pressure largely varied during the production run. Therefore, the data of the downward set below 600 K are omitted in Fig. 5.1(a) and so on.

In the Li_2O upward set, on the other hand, while Li shows large self-diffusion coefficients comparable with that in the super-cooled liquid state, O shows much lower values than that in the super-cooled liquid state. This result suggests that the crystalline phase of Li_2O is partially melted in the upward set, which is so-called superionicity of Li as previously observed in experiments [50], [51] and in MD simulations [50], [52]. Thus, we consider that the superionic transition temperature T_c is around 800 K with the present potential model. This temperature is consistent with an empirical fact that the superionic transition temperature is usually 0.6-0.8 times of the melting temperature [21].

Regarding the MS diffusion coefficients, Eq. (4.2) provides approximate values that reasonably agree with exact values calculated with Eq. (3.38) in Figs. 5.2. In Fig. 5.2(a) for Li_2O, where the self-diffusion coefficients are largely different between the two components, the MS diffusion coefficient basically resides between the two self-diffusion coefficients for the low temperatures, as can be expected from Eq. (4.2). However, as the temperature increase, the MS diffusion coefficient cut through the lower bound (self-diffusion coefficient of Oxygen in Fig. 5.2(a)) showing the smaller value. This trend is also observable in Fig. 5.2(b) for TiO_2. The common reason for this trend is due to the transition from the ideal to the realistic behavior of inter-diffusion coefficient.

As an one type of inter-diffusion coefficient, the MS diffusion coefficient shows an ideal behavior at the low temperatures, where the interactions between the atoms are not so severe. From the definition of MS diffusion coefficient in Eq. (3.36) and so on, it can be noticed that the consideration of velocity correlation between distinct atoms is included via $Ł_{kl}$. Here, the cross correlation between distinct atoms should be negligible for the low temperatures, resulting in the fair agreement between $Đ_{12}^{approx.}$ and $Đ_{12}$. However, as the temperature increases, atoms become more mobile, mixing up with each other more randomly. This leads to a sort of friction between interacting atoms, showing less $Đ_{12}$ value than the $Đ_{12}^{approx.}$.

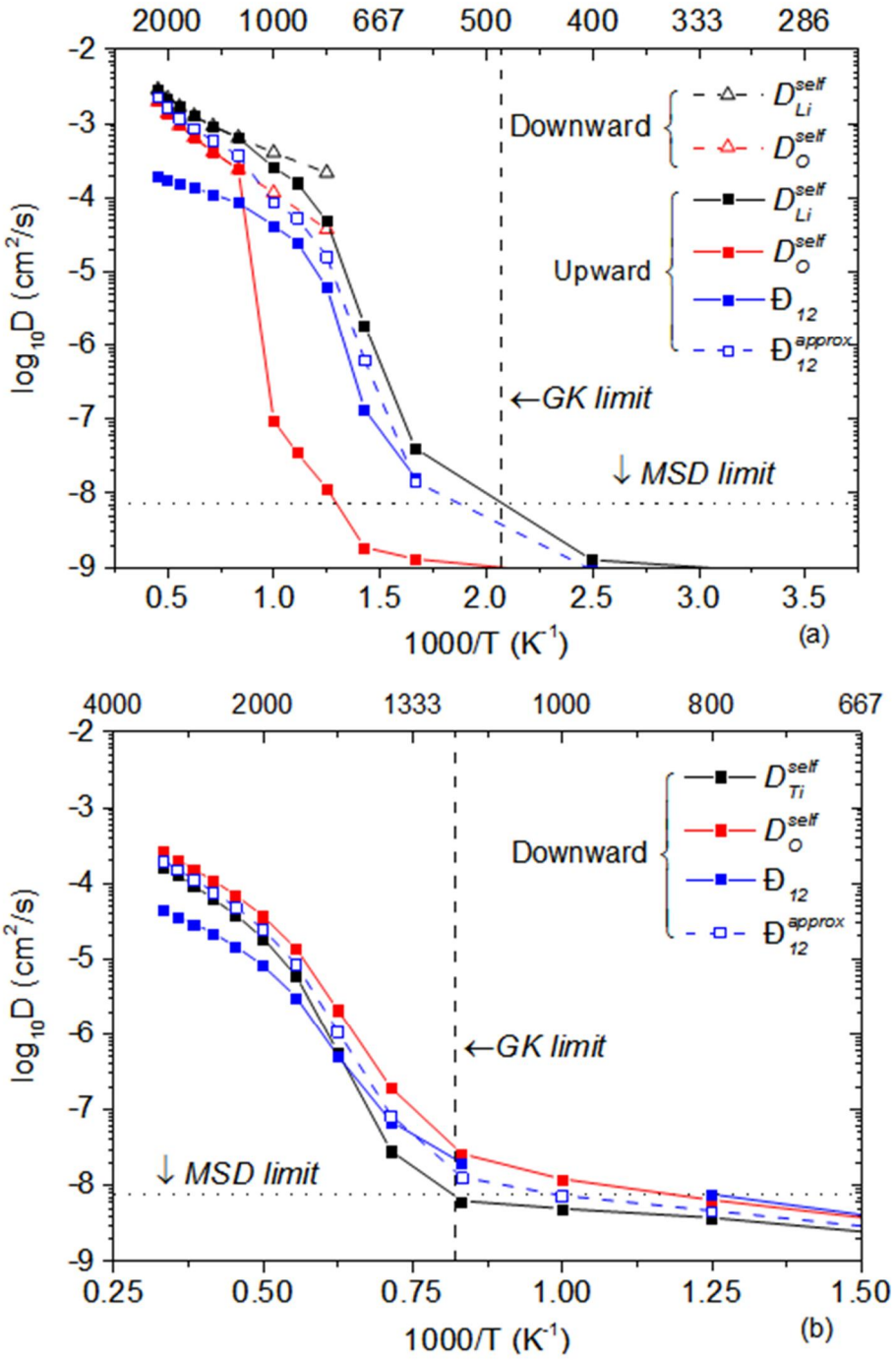

Figure. 5.2 Arrhenius plot of diffusion coefficients (a) Li_2O and (b) TiO_2.

5.1.2 TiO_2 Model system

The simulations results for TiO_2 model systems are shown in Fig 5.1(b) and Fig 5.2(b). For the upward set in Fig 5.1(b), the melting did not occur up to 3000 K, while the experimental melting point of TiO_2 is 2128 K [53]. This is because the upward set is prone to overestimate the melting point. To determine the melting point exactly, we again conducted the simulation of coexisting phases and confirmed that the melting point of the present potential model is between 2900 and 3000 K. Thus, the phase appeared in the upward set is solely crystalline solid. In Fig. 5.2(b), the diffusion coefficient data of upward set of TiO_2 is omitted, as the value of diffusion coefficients are always far lower than the statistical limits (both MSD and GK limits) set in this study.

Upon quenhing from the liquid state, TiO_2 is known as a material to show the glass-transition [54]. In the downward set in Fig. 5.1(b), the glass transition is indicated at around 1500 K as a slope change in the temperature dependence of the volume. The glass transition is also confirmed with large self-diffusion coefficients like those in a liquid ($D^{self} \approx 10^{-6}$ cm^2/s) after around 1500 K in Fig. 5.2(b).

To sum up, Fig. 5.3 summarizes the phases observed in simulations.

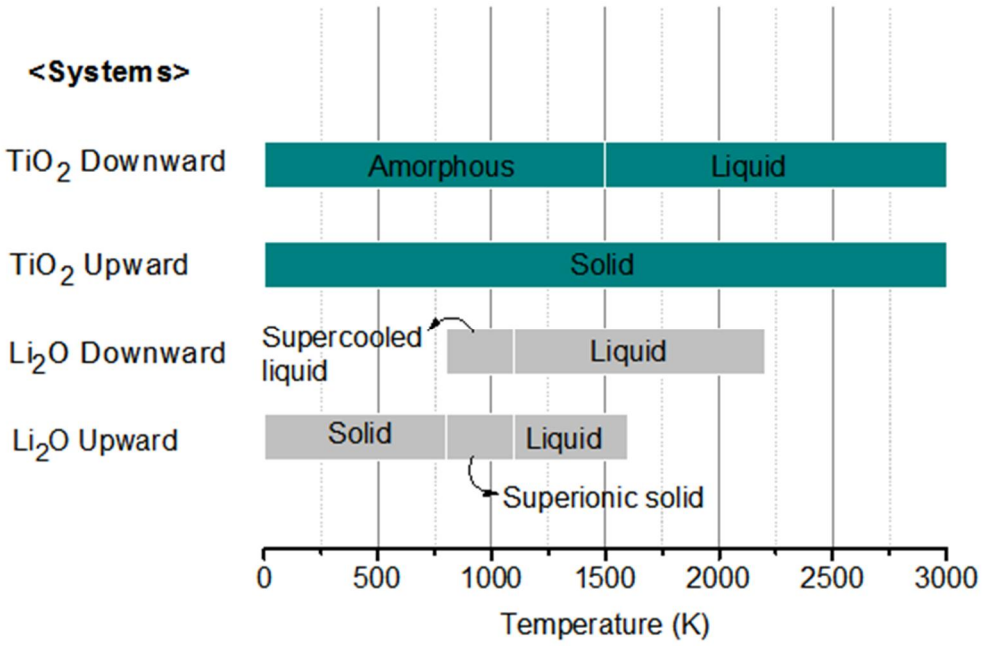

Figure. 5.3 Summary of phases observed in the MD simulations.

5.2 Thermal conductivity

5.2.1 Li_2O Model system

Figure 5.4 shows the TC values of Li_2O model systems, together with experimental values [55], [56]. There, κ_1 and κ_2 show virtually identical values. They decrease inversly proportional to the temperature increase. This decreasing trend is a typical temperature dependence of the dielectric materials, which is well-explained by the umklapp scattering of phonon [57], and is comparable with the experimental results. The decreasing slope becomes moderate at around T_c and T_m, which is also a typical temperature dependence for materials of disordered states. Noticeably, κ_1^* starts to deviate from κ_1 and κ_2 at around T_c. As the temperature increases even more, κ_1^* holds comparable values with κ_1 and κ_2.

For the downward set, only two data points of κ_1^* at 800 K and 900 K are given in Fig. 5.4, where the phase of system was verified as the super-cooled liquid state. It was because the results in the downward set are basically the same with results in the upward set except for these two temperature points, due to the identical phase status. Here, κ_1^* shows larger deviations from κ_1 and κ_2 in the downward set than that in the upward set at 800 K and 900 K. This observation implies that the deviation of κ_1^* may depend on the degree of mobility of atoms in the system.

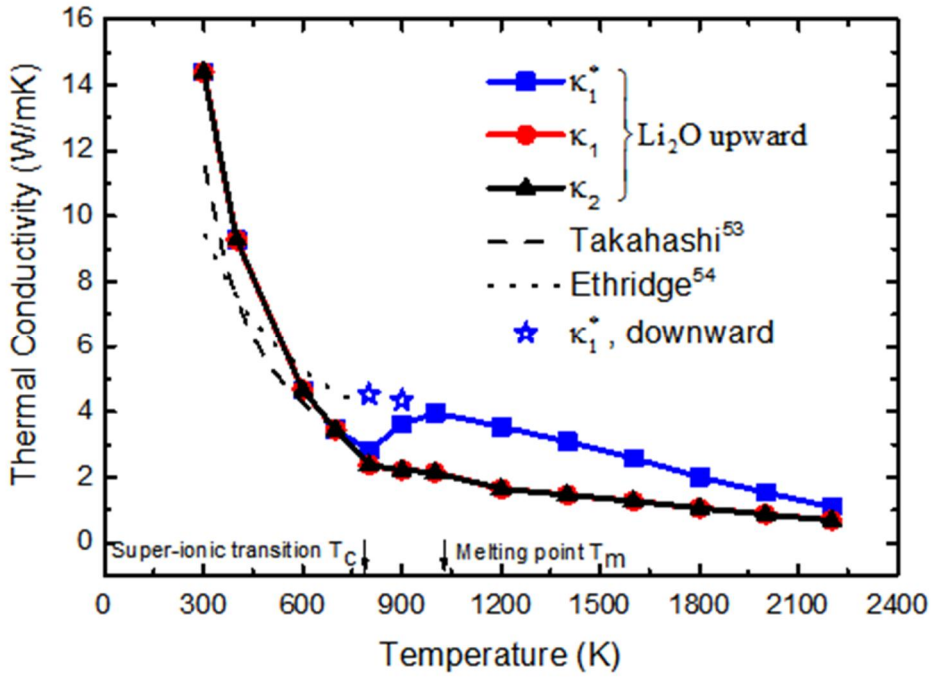

Figure. 5.4 Thermal conductivity results of Li_2O by EMD with various thermal conductivity expressions, together with the experimental value [55], [56].

5.2.2 TiO_2 Model system

Figures 5.5 and 5.6 show the TC values of TiO_2 model system of the upward and downward sets, respectively, together with experimental values [57] in Fig. 5.5. Because there are no substantial differences among the three TC expressions in the TiO_2 upward set, only κ_2 values are given in Fig. 5.5. Such a fair correspondance between different TC expressions can be inferred from Eqs. (3.40) and (3.42), as the diffusion coefficients are low in TiO_2 upward systems. As the rutile structure has an anisotropy between the a-axis and the c-axis, TC in parallel to the c-axis is different from that perpendicular to the c-axis. Both parallel and perpendicular TCs show again the ordinary temperature dependence of dielectric materials, which is inversly proportional to the temperature. Although the agreement between the simulation and the experiment is more of less poor, we consider that this disagreement is still acceptable for the purpose of the present study.

As can be seen in Fig. 5.6, the TCs obtained in the downward set (of a disordered phase) are always lower than those obtained in the upward set (of an ordered phase). In similar to the results of Li_2O, κ_1 and κ_2 hold virtually identical values for the overall temperature range, while κ_1^* deviates from them above 1600 K. Note that this 1600 K is sufficiently higher than the GK limit of TiO_2 downward set (1200 K), suggesting that there is a temperature range where the diffusion vigorously occurs but all three TC expressions show practically identical values.

In addition, test results on the system size effect are given in Fig. 5.6, where 4×4×6 and 9×9×12 supercells were additionally used. Comparable results were obtained in the three different cells, confirming that the 6×6×9 supercell is big enough to avoid the system size effect.

In summary, κ_1 and κ_2 are all the same for any conditions and systems, while κ_1^* shows erroneous values at some high temperatures. The conditions where κ_1^* deviates from κ_1 and κ_2 are closely related to the superionic-transition and the glass-transition respectively for Li_2O and TiO_2, as well as the melting. These phase transitions correspond to the emergence of phases of high atomic mobility. As analytically proven in Eqs. (3.40) and (3.42), the MS diffusion coefficient is a key factor to determine the differences among the three TC expressions. Therefore, it is reasonable that the error in κ_1^* depends on the atomic mobility. However, since there are two other factors ($\Delta\bar{h}$ and $\bar{Q}_1$) that are involved in Eqs. (3.40) and (3.42), it is still not clear which factor mainly triggers the error in κ_1^*. In the next section, we will show calculation results of $\Delta\bar{h}$ and $\bar{Q}_1$ for the further analysis.

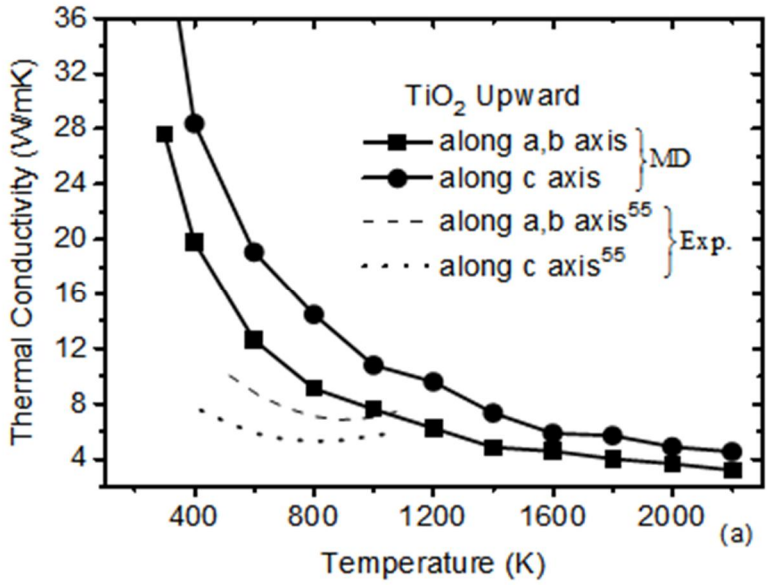

Figure. 5.5 TC result of TiO_2 upward for parallel and perpendicular to c-axis of the rutile, together with the experimental value [57]

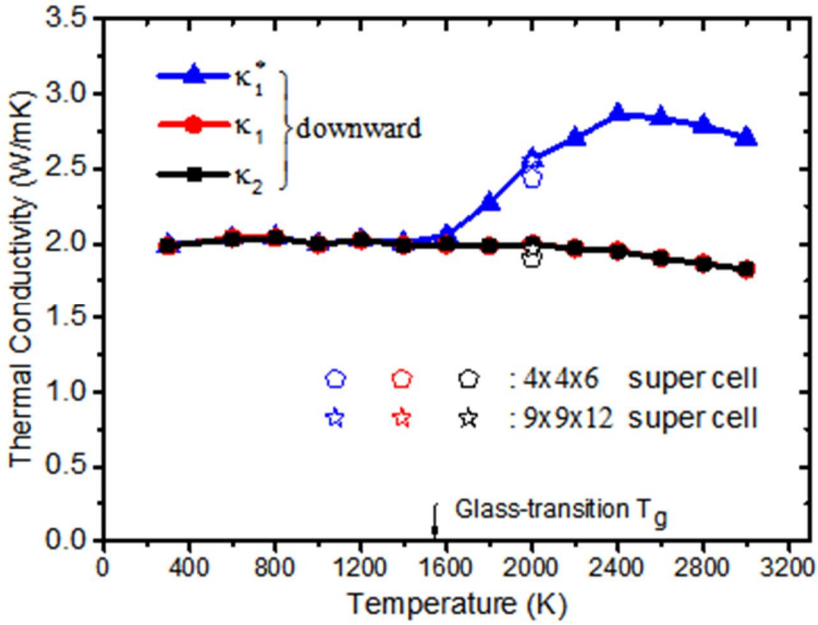

Figure. 5.6 TC result of TiO_2 downward.

5.2.3 The difference of partial specific enthalpy, $\Delta\bar{h}$

Figure. 5.7(a) shows the temperature dependence of the absolute value of $\Delta\bar{h}$. In Li_2O, the superionic transition at 800 K does not largely affect $\Delta\bar{h}$, while the melting at 1100 K does so. This is because the superionic transition in an (anti-)fluorite crystal such as UO_2 and Li_2O is a second-order phase transition [58], [59] where the enthalpy changes continuously, while the melting is a first-order phase transition where it changes discontinuously.

For the TiO_2 upward set, $\Delta\bar{h}$ monotonically increases because the system does not go through any phase transition. In the downward set, $\Delta\bar{h}$ non-monotonically changes due to the grass transition. Nevertheless, unlike the volume and diffusion coefficients, the value of $\Delta\bar{h}$ is rather insensitive to temperature in general, showing at most 20% difference from the value at 0 K over 0 - 3000 K. Because of this weak temperature dependence, the $\Delta\bar{h}$ value estimated at 0 K can represent $\Delta\bar{h}$ value for any temperature with a reasonable accuracy.

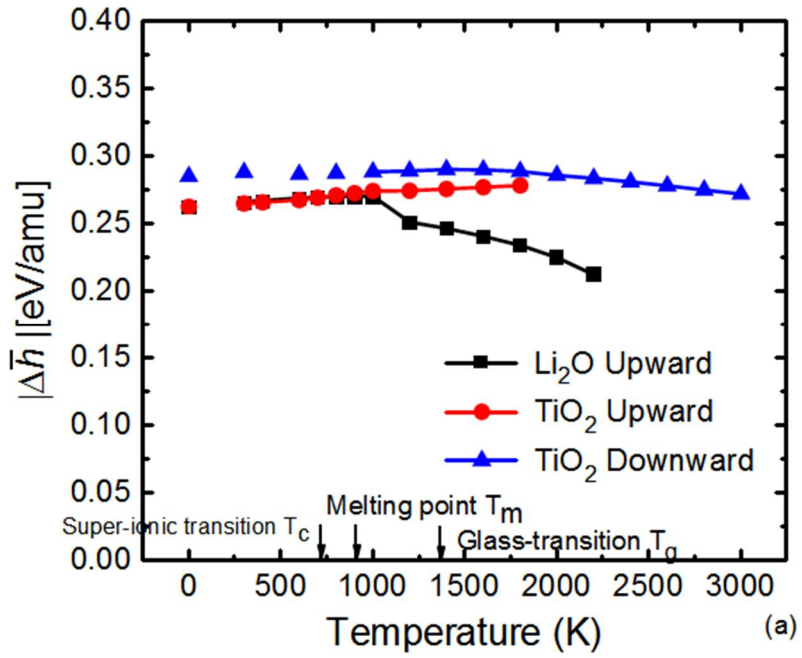

Figure. 5.7 Temperature dependence of the difference of partial specific molar enthalpy $\Delta\bar{h}$ ..

5.2.4 The reduced heat of transport, $\bar{Q}_1$

Figure. 5.8 shows the temperature dependence of $\bar{Q}_1$, which was calculated by averaging two $\bar{Q}_1$ values deduced from L_{1Q}/L_{11} and L_{Q1}/L_{11}. The relation between $\bar{Q}_1$ and $\bar{Q}_2 = L_{2Q} / L_{22}$ is given as $\bar{Q}_1 = -\bar{Q}_2$ under the condition of fixed center of mass. The calculated $\bar{Q}_1$ values seem to be erroneous at temperatures around and below the GK limit for both Li_2O and TiO_2, which is consistent with the discussion in section 4.2.2. At temperatures higher than the GK limit, it is expected that L_{1Q}/L_{11} and L_{Q1}/L_{11} are virtually the same according to the Onsager's reciprocal relation [32]. As shown in Table. 5.1, however, the mismatch between L_{1Q}/L_{11} and L_{Q1}/L_{11} is still large up to 1600 K due to statistical errors. In general, much larger computational cost is required for accurate determination of cross PCs compared to direct PCs, because cross phenomena are more rare and have weaker correlation than the direct phenomena. Therefore, a longer simulation time than the present setting is needed to achieve a better consistency between L_{1Q}/L_{11} and L_{Q1}/L_{11}. Nonetheless, we consider that the accuracy of $\bar{Q}_1$ in Fig. 5.8 is acceptably high for the purpose of the present study, because we can still confirm with the present results that the effect of $\bar{Q}_1$ on TC is suppressed due to negligible MS diffusion coefficients at low temperatures and due to small absolute values of $\bar{Q}_1$ itself at high temperatures.

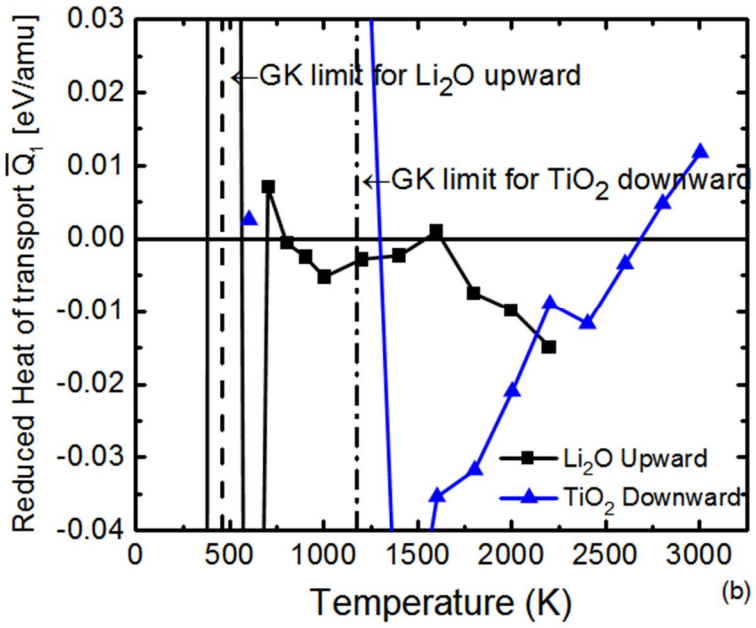

Figure. 5.8 Temperature dependence of the reduced heat of transport $\bar{Q}_1$.

Table. 5.1 Comparison of the reduced heat of transport by L_{1Q}/L_{11} and L_{Q1}/L_{11} for TiO_2 downward (eV/amu).

Temp. (K)	L_{1Q}/L_{11}	L_{Q1}/L_{11}
300	-0.687	0.433
600	-0.516	0.521
800	-0.041	0.122
1000	0.288	0.178
1200	0.015	0.110
1400	0.022	-0.156
1600	-0.004	-0.067
1800	-0.038	-0.026
2000	-0.016	-0.026
2200	-0.011	-0.007
2400	-0.007	-0.016
2600	-0.004	-0.002
2800	0.007	0.003
3000	0.013	0.011

Both $\bar{Q}_1$ and $\Delta\bar{h}$ are parameters to affect differences among the three TC expressions as shown in Eqs. (3.40) and (3.42). Compared to $\Delta\bar{h}$, $\bar{Q}_1$ holds around one order of magnitude smaller absolute values. As a result, the PSE effect becomes a dominant cause of differences in the three TC expressions for both Li_2O and TiO_2.

Regarding the temperature response, $\bar{Q}_1$ the TiO_2 downward set shows a positive temperature dependence at low temperatures, and changes its sign from negative to positive at around 2700 K. This inversion of sign denotes the fact that the moving direction of component 1 with respect to the temperature gradient changes at around 2700 K. As TiO_2 is an ionic system, their mass current corresponds directly to the electric current, and thus should have a one-way current direction. This is so-called the thermoelectric phenomenon. The inversion of the sign of $\bar{Q}_1$ at around 2700 K is thus interpreted as a change in the direction of electric current. We do not further analyze the physical significance of this result because it is not necessarily needed for the purpose of the present study.

Chapter 6. Discussion

6.1 Temperature dependence of TC differences

6.1.1 Li_2O Model system

The temperature dependences of $\kappa_1^* - \kappa_1$ and $\kappa_1 - \kappa_2$ in Li_2O upward set are shown in Fig. 6.1. Their absolute values are depicted with the connected lines. The square box graph represents the ratio of each error term with respect to κ_2, which were calculated by dividing the 1st and 2nd terms of $\kappa_1^* - \kappa_1$ in Eq. (3.42) with κ_2. Note that as we decided the reference TC value as κ_2, the discussion of "error" of TC value should be made with respect to κ_2 to be consistent. However, since κ_1 shows the same value with κ_2 in the current model systems, $\kappa_1^* - \kappa_2$ is equivalent with $\kappa_1^* - \kappa_1$. Thus, it is possible to simply consider $\kappa_1^* - \kappa_1$ in Fig. 6.1 as the error of κ_1^*.

In Fig. 6.1, κ_1^* starts to deviate from κ_2 above 800 K. κ_1^* exhibits a maximum error of 1.9 W/mK at 1200 K, and then decreases steadily. The maximum error corresponds to 120% error with respect to κ_2. The error ratio graph indicates that only the 2nd term of κ_1^* error has a meaningful value, which is the PSE effect, as expected from the result in section 5.2.4.

The error of κ_1^* shows a non-monotonic response to the temperature. This complex temperature dependence comes from different temperature dependences of the MS diffusion coefficient and the volume. As a simplified mathematical model, let us assume that the system volume changes in proportion to T^m with m = 1~1.5, which was roughly estimated from Figs. 5.1, and that the MS diffusion coefficient follows a typical Arrhenius equation. Because the temperature dependence of κ_1^* error comes from temperature dependences of 3 terms (T, V, and $Đ_{12}$), $\kappa_1^* - \kappa_1$ has $\sim \exp(-E_d / k_B T) / T^{m+2}$ dependence, where E_d is the effective activation energy for the MS diffusion coefficient. This function has a local minimum at a positive T value. In other words, even though the MS diffusion coefficient increases according to the Arrhenius equation, it is soon overwhelmed by the temperature dependence of the denominator of $\kappa_1^* - \kappa_1$ in Eq. (3.42), which increases as T^{m+2} with m = 1~1.5.

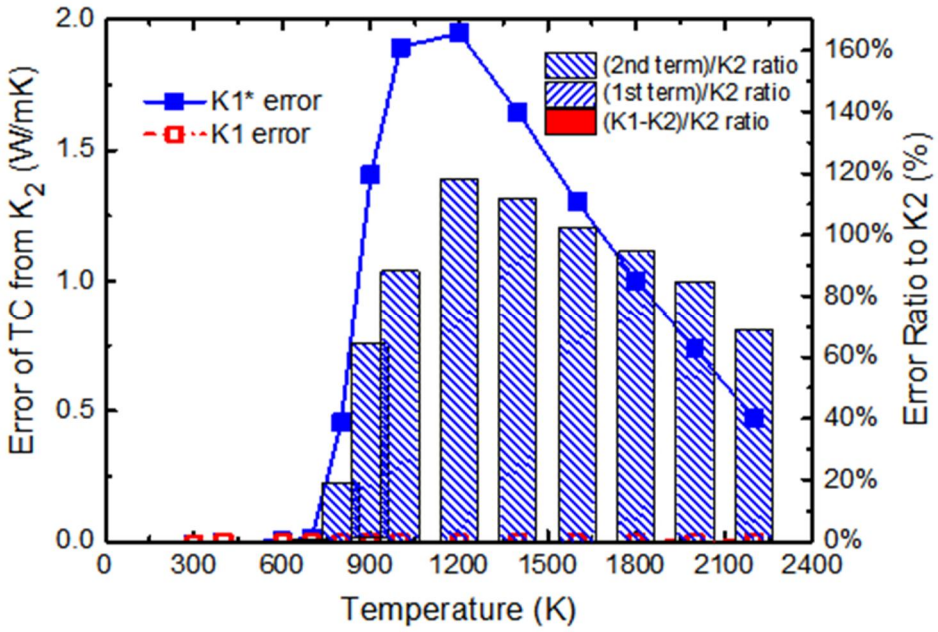

Figure. 6.1 Comparison of lattice TC expressions for Li_2O by (a) the absolute value and (b) ratio

6.1.2 TiO_2 Model system

Temperature dependences of $\kappa_1^* - \kappa_1$ and $\kappa_1 - \kappa_2$ in TiO_2 downward set are shown in Fig. 10. As previously seen, κ_1^* starts to deviate from κ_2 above 1600 K, which is just after the glass-transition temperature of around 1500 K. κ_1^* exhibits a maximum error of 1.0 W/mK at 2600 K, which corresponds to around 60% error with respect to κ_2. Again, it is turned out that only the 2nd term of the error of κ_1^* given by Eq. (3.42), namely the PSE effect, has the meaningful value.

The error of κ_1^* also shows a non-monotonic response to temperature in TiO_2 downward set like in Li_2O systems. However, the responses are somewhat different between them. This is because the volume expansion is more moderate in the TiO_2 downward set than that in the Li_2O upward set. As the volume term suppress the error of κ_1^*, a moderate thermal expansion of a system makes the κ_1^* error last longer at higher temperatures. Thus it is expected that materials with smaller thermal expansion will suffer a larger error by using κ_1^*.The superionic transition materials including various oxide compounds, for example, can correspond to such candidate group as the sub-lattice of superionic conductors is persistent to the severe thermal expansion while the fast-conducting ions exist.

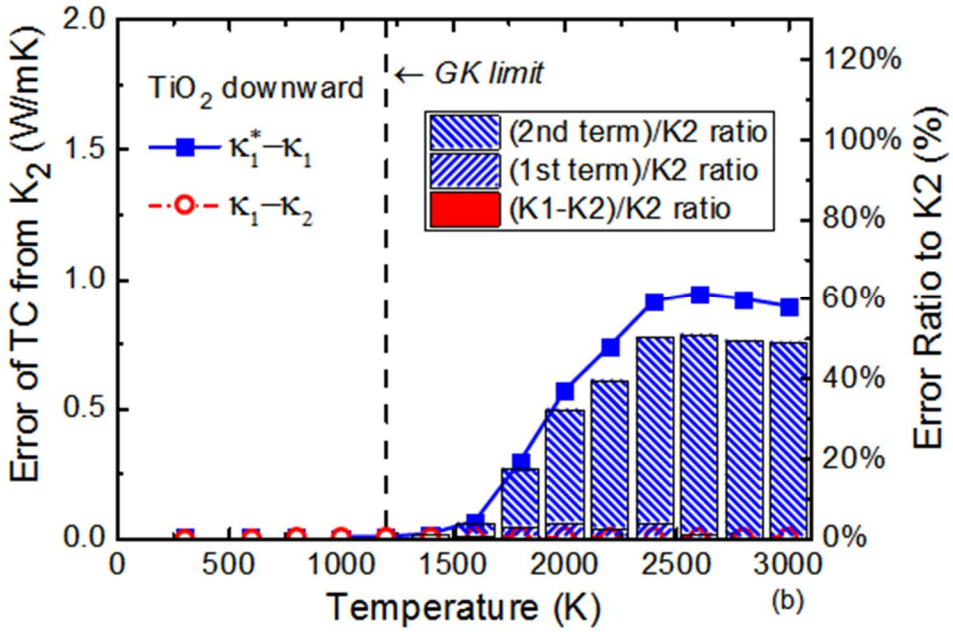

Figure. 6.2 Comparison of TC expressions, for TiO_2 downward by the absolute value and ratio.

6.2 Comparison among PSE, Cross and PSE-Cross effects

To sum up the results of Li_2O and TiO_2, the onset of κ_1^* error is closely related to the degree of mobility of atoms, which is represented by the MS diffusion coefficient. Even though κ_1^* error also depends on $\Delta\bar{h}$ and $\bar{Q}_1$, their temperature responses are negligibly small compared to the temperature dependence of MS diffusion coefficient, which varies more than several orders of magnitude. Therefore we can approximately consider that the effects of $\Delta\bar{h}$ and $\bar{Q}_1$ in the κ_1^* error are temperature-independent constants.

For both Li_2O and TiO_2 systems, the PSE effect overwhelms both the Cross effect and the PSE-Cross effect, due to a relatively small values of $\bar{Q}_1$. In previous studies, however, there is a report of a relatively large $\bar{Q}_1$ value, such as 0.25 eV for hydrogen impurity in palladium [22], which is comparable with $\Delta\bar{h}$ in the present study. However, this is a case of dilute impurity, not a case of constituent atom. As far as we searched, there is no previous study that reports a large $\bar{Q}_1$ value for a constituent element. Consequently, we may suggest that for binary systems composed of both of constituent atoms, the Cross effect and the PSE-Cross effect are basically negligible. However for the binary systems of impurity-containing systems,

one may seriously consider the possibility of the occurrence of Cross and PSE-Cross effect.

6.3 Simple method to approximately evaluate the error in κ_1^*

When the κ_1^* error starts to occur, the value of MS diffusion coefficient is about 4×10^{-6} cm^2/s in the Li_2O upward set and 5×10^{-7} cm^2/s in the TiO_2 downward set. According to the approximate relation between the MS diffusion coefficient and the self-diffusion coefficient given by Eq. (4.2), the self-diffusion coefficient of 10^{-6} cm^2/s can be employed as an indicator of the onset of a significant error in κ_1^*. Because 10^{-6} cm^2/s is a typical diffusion coefficients around the melting point, a significant error of κ_1^* is expected to occur at around and above the melting point for binary systems, and at some lower temperatures for superionic transition materials. A defective system, where a diffusion is usually enhanced by defects, may also suffer a significant error of κ_1^* even in a solid phase.

A possible error of κ_1^* can be roughly estimated as follows:

$$
\begin{aligned}
\kappa_1^* - \kappa_1 &= \left(2\Delta\bar{h}\cdot\bar{Q}_1 + (\Delta\bar{h})^2\right)\frac{Nm_1^2}{Mk_BVT^2}Đ_{12} \\
&\sim (\Delta\bar{h})^2\frac{Nm_1^2}{Mk_BVT^2}Đ_{12} \\
&\sim (\Delta\bar{h}_{0K})^2\frac{Nm_1^2}{Mk_BVT^2}Đ_{12} \\
&\sim (\Delta\bar{h}_{0K})^2\frac{Nm_1^2}{Mk_BVT^2}\left(x_2D_1 + x_1D_2\right),
\end{aligned}
\tag{6.1}
$$

where we first neglect the PSE-Cross effect, second replace $\Delta\bar{h}$ with $\Delta\bar{h}$ at 0 K ($\Delta\bar{h}_{0K}$), and third replace $Đ_{12}$ with $Đ_{12}^{approx.}$. If a significant value is indicated by Eq. (6.1), it is recommended that κ_1 or κ_2 is used instead of κ_1^* for accurate evaluation of the TC.

6.4 Effect of pv term in the definition of $\Delta\bar{h}$

Finally, we would like to emphasize the important of using correct $\Delta\bar{h}$ is in the calculation of κ_1 . As the determination of PSE is known as a difficult task [13], [60], it is worthwhile to see an example of one result with an inappropriate $\Delta\bar{h}$ value. Let us take the TiO_2 downward set as a test case, where we approximately replace $\Delta\bar{h}$ with $\Delta\bar{u} = \bar{u}_1 - \bar{u}_2$ by neglecting the pV term in Eq. (3.25). As a result of this test, $\Delta\bar{h}$ and $\bar{Q}_1$ are wrongly obtained as around 0.1 eV and 0.2 eV, respectively. This is a natural consequence according to the relation of Eq. (3.32) because the correct $\Delta\bar{h}$ value is around 0.3 eV and $\bar{Q}_1$ is negligibly small.

Figure 6.3 shows the result of this test. The Cross effect is no longer negligible due to the wrong $\Delta\bar{h}$ value. In addition, the 1st term in $\kappa_1^* - \kappa_1$ becomes also non-negligible. This test calculation suggests that a careful attention is requested on the determination of $\Delta\bar{h}$ value when using κ_1 as the TC expression. Meanwhile, κ_2 can serve as an ever-safe choice of TC.

However, as for κ_2 , its expression becomes complicated as the number of components increases: see a ternary case in Ref. [61]. Moreover, in a system containing defects, the determination of $\Delta\bar{h}$ as well as writing down of the κ_2 expression becomes more difficult. This is because defects differ the energies of atoms even of the same element, and thus the averaged

PSE can no longer appropriately represent the average energy of each atom of the same element. As a result, some atoms of the same element need to be considered as different chemical species form others. Similar consideration on the difficulty on the PSE determination has been noted by Babaei *et al*. [33]. In such a situation, κ_1^* expressions may be recommended as far as the application is limited to a system where components have low diffusion coefficients. However, when defects are contained, diffusion coefficients are usually enlarged by defect-assisted diffusion mechanism. Therefore, a careful analysis is needed in the application of the GK relation to a defective system, which is another important research topic for future works.

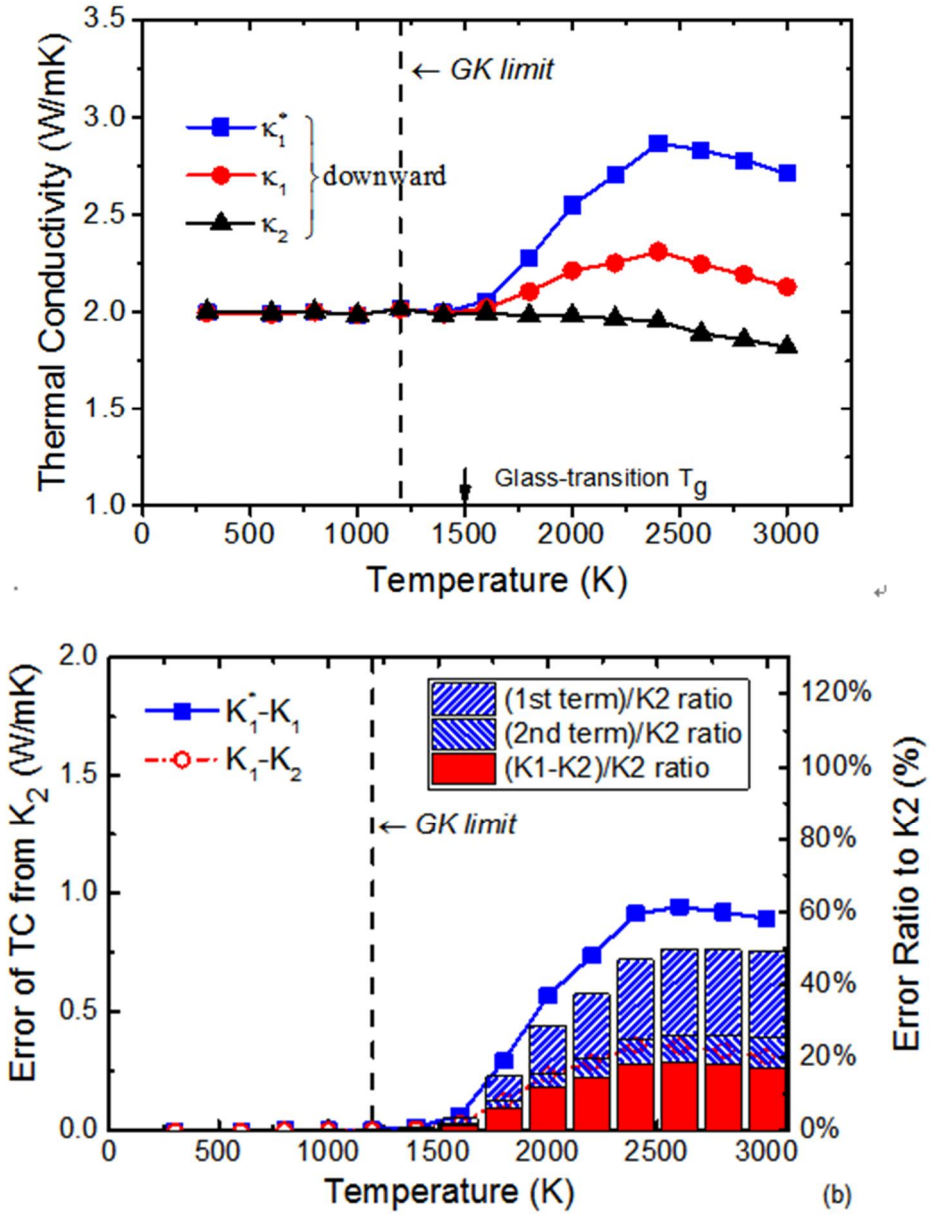

Figure. 6.3 (a) TC result of TiO_2 downward with the approximation of $\Delta\bar{h}$ as $\Delta\bar{u}$, and (b) the error of TC expressions by its absolute value and ratio with respect to κ_2.

Chapter 7. Conclusion

In the present study, we first reviewed the concurrent existing TC expressions used in EMD, which vary with each other. The major reason for the different formalism is investigated starting from the equation of entropy production. Consequently, κ_2 is suggested as the reference TC expression for the binary systems because it requires the least assumptions to justify its derivation. Therefore, we referred to the value of κ_2 for the discussion of the accuracy of other TC expressions. As examples, Li_2O and TiO_2 model systems are tested including their disordered phases to confirm the resultant differences between various TC expressions, and to find out the key factors that trigger these differences. The results suggest that κ_1^* results in the error of at most 120% for Li_2O, and 60% for TiO_2 compared to the κ_2 value, and that MS diffusion coefficient is the decisive parameters which triggers the error of TC.

With comparison to other two expressions (κ_1 and κ_1^*), it is revealed that κ_2 is obtained by subtracting the contribution of energy transport via mass diffusion from the overall energy transport. Thus the remaining part of κ_2 represents the purely conductive process of excess energy, which is heat. The subtracted energy is composed of two kinds of characteristic energy of a material; the difference of PSE and reduced heat of transport. They are one

of the important components for the error of TC. Nevertheless, without sufficiently high value of the MS diffusion coefficient, the error of TC can be invisible even with using inappropriate TC expressions. For a simple estimation of TC error, we suggest to use the value of self-diffusion coefficient and the value of $\Delta\bar{h}$ which can be simply obtained by static calculation. Furthermore, we put forward that a binary system containing light-element impurity might be dangerous to use even κ_1, as the $\bar{Q}_1$ value is expected to have comparable value to $\Delta\bar{h}$.

Bibliography

[1] W. J. Parker, R. J. Jenkins, C. P. Butler, and G. L. Abbott, "Flash Method of Determining Thermal Diffusivity, Heat Capacity, and Thermal Conductivity," *J. Appl. Phys.*, vol. 32, no. 9, pp. 1679–1684, Sep. 1961.

[2] J. E. Turney, E. S. Landry, A. J. H. McGaughey, and C. H. Amon, "Predicting phonon properties and thermal conductivity from anharmonic lattice dynamics calculations and molecular dynamics simulations," *Phys. Rev. B*, vol. 79, no. 6, p. 64301, Feb. 2009.

[3] A. J. H. McGaughey and M. Kaviany, "Quantitative validation of the Boltzmann transport equation phonon thermal conductivity model under the single-mode relaxation time approximation," *Phys. Rev. B*, vol. 69, no. 9, p. 94303, Mar. 2004.

[4] J. Eapen, J. Li, and S. Yip, "Mechanism of Thermal Transport in Dilute Nanocolloids," *Phys. Rev. Lett.*, vol. 98, no. 2, p. 28302, Jan. 2007.

[5] S. Sarkar and R. P. Selvam, "Molecular dynamics simulation of effective thermal conductivity and study of enhanced thermal transport mechanism in nanofluids," *J. Appl. Phys.*, vol. 102, no. 7, p. 74302, 2007.

[6] D. MacGowan and D. J. Evans, "Heat and matter transport in binary liquid mixtures," *Phys. Rev. A*, vol. 34, no. 3, pp. 2133–2142, Sep. 1986.

[7] G. D. Samolyuk, S. I. Golubov, Y. N. Osetsky, and R. E. Stoller, "Molecular dynamics study of influence of vacancy types defects on thermal conductivity of β-SiC," *J. Nucl. Mater.*, vol. 418, no. 1–3, pp. 174–181, Nov. 2011.

[8] J. W. Lawson, M. S. Daw, and C. W. Bauschlicher, "Lattice thermal conductivity of ultra high temperature ceramics ZrB2 and HfB2 from atomistic simulations," *J. Appl. Phys.*, vol. 110, no. 8, p. 83507, 2011.

[9] P. K. Schelling, S. R. Phillpot, and P. Keblinski, “Comparison of atomic-level simulation methods for computing thermal conductivity,” *Phys. Rev. B*, vol. 65, no. 14, p. 144306, Apr. 2002.

[10] Z. Fan, L. F. C. Pereira, H.-Q. Wang, J.-C. Zheng, D. Donadio, and A. Harju, “Force and heat current formulas for many-body potentials in molecular dynamics simulations with applications to thermal conductivity calculations,” *Phys. Rev. B*, vol. 92, no. 9, p. 94301, 2015.

[11] A. Guajardo-Cuéllar, D. B. Go, and M. Sen, “Evaluation of heat current formulations for equilibrium molecular dynamics calculations of thermal conductivity,” *J. Chem. Phys.*, vol. 132, no. 10, p. 104111, 2010.

[12] T. Arima, K. Yoshida, T. Matsumoto, Y. Inagaki, and K. Idemitsu, “Thermal conductivities of ThO2, NpO2 and their related oxides: Molecular dynamics study,” *J. Nucl. Mater.*, vol. 445, no. 1–3, pp. 175–180, 2014.

[13] N. Galamba, C. A. Nieto de Castro, and J. F. Ely, “Equilibrium and nonequilibrium molecular dynamics simulations of the thermal conductivity of molten alkali halides.,” *J. Chem. Phys.*, vol. 126, no. 20, p. 204511, 2007.

[14] N. Galamba, C. A. Nieto de Castro, and J. F. Ely, “Thermal conductivity of molten alkali halides from equilibrium molecular dynamics simulations,” *J. Chem. Phys.*, vol. 120, no. 18, p. 8676, 2004.

[15] S. Nichenko and D. Staicu, “Molecular Dynamics study of the effects of non-stoichiometry and oxygen Frenkel pairs on the thermal conductivity of uranium dioxide,” *J. Nucl. Mater.*, vol. 433, no. 1–3, pp. 297–304, 2013.

[16] T. Ouyang, X. Zhang, and M. Hu, “Thermal conductivity of ordered-disordered material: a case study of superionic Ag 2 Te,” *Nanotechnology*, vol. 26, no. 2, p. 25702, Jan. 2015.

[17] P. J. D. Lindan and M. J. Gillan, “A molecular dynamics study of the thermal conductivity of CaF 2 and UO 2,” *J. Phys. Condens. Matter*, vol. 3, no. 22, pp. 3929–3939, Jun. 1991.

[18] P. Sindzingre and M. J. Gillan, “A computer simulation study of transport coefficients in alkali halides,” *J. Phys. Condens. Matter*, vol. 2, pp. 7033–7042, 1990.

[19] M. S. Green, “Markoff Random Processes and the Statistical Mechanics of Time-Dependent Phenomena. II. Irreversible Processes in Fluids,” *J. Chem. Phys.*, vol. 22, no. 3, p. 398, 1954.

[20] R. Kubo, “The fluctuation-dissipation theorem,” *Reports Prog. Phys.*, vol. 29, no. 1, p. 306, Jan. 1966.

[21] S. Hull, “Superionics: crystal structures and conduction processes,” *Reports Prog. Phys.*, vol. 67, no. 7, pp. 1233–1314, Jul. 2004.

[22] P. K. Schelling and T. Le, “Computational methodology for analysis of the Soret effect in crystals: Application to hydrogen in palladium,” *J. Appl. Phys.*, vol. 112, no. 8, p. 83516, 2012.

[23] B. Bernu and J. P. Hansen, “Thermal Conductivity of a Strongly Coupled Hydrogen Plasma,” *Phys. Rev. Lett.*, vol. 48, no. 20, p. 1375, 1982.

[24] Y. Lee, R. Biswas, C. Soukoulis, C. Wang, C. Chan, and K. Ho, “Molecular-dynamics simulation of thermal conductivity in amorphous silicon,” *Phys. Rev. B*, vol. 43, no. 8, pp. 6573–6580, 1991.

[25] W. C. Tucker, L. Shokeen, and P. K. Schelling, “Atomic-scale simulation of the thermodiffusion of hydrogen in palladium,” *J. Appl. Phys.*, vol. 114, no. 6, p. 63509, 2013.

[26] G. Guevara-Carrion, T. Janzen, Y. M. Muñoz-Muñoz, and J. Vrabec, “Mutual diffusion of binary liquid mixtures containing methanol, ethanol, acetone, benzene, cyclohexane, toluene, and carbon tetrachloride,” *J. Chem. Phys.*, vol. 144, no. 12, p. 124501, Mar. 2016.

[27] C. Hoheisel, *Theoretical treatment of liquids and liquid mixtures*, 1st ed. Elsevier, 1993.

[28] D. A. McQuarrie and J. D. Simon, *Physical Chemistry: A Molecular Approach*, no. V. 1. University Science Books, 1997.

[29] S. R. de Groot and P. Mazur, *Non-equilibrium Thermodynamics*. Dover Publications, 1984.

[30] F. Bresme, B. Hafskjold, and I. Wold, “Nonequilibrium Molecular Dynamics Study of Heat Conduction in Ionic Systems,” *J. Phys. Chem.*, vol. 100, no. 5, pp. 1879–1888, Jan. 1996.

[31] J. M. Ziman, *Electrons and Phonons: The Theory of Transport Phenomena in Solids*. Clarendon Press, 1960.

[32] L. Onsager, “Reciprocal Relations in Irreversible Processes. I.,” *Phys. Rev.*, vol. 37, no. 4, pp. 405–426, 1931.

[33] H. Babaei, P. Keblinski, and J. M. Khodadadi, “Equilibrium molecular dynamics determination of thermal conductivity for multi-component systems,” *J. Appl. Phys.*, vol. 112, no. 5, p. 54310, 2012.

[34] H. J. M. Hanley, *Transport phenomena in fluids*. M. Dekker, 1969.

[35] C. Chen, H. Y. Hsiao, Y. W. Chang, F. Ouyang, and K. N. Tu, “Thermomigration in solder joints,” *Mater. Sci. Eng. R Reports*, vol. 73, no. 9–10, pp. 85–100, 2012.

[36] W. C. Tucker and P. K. Schelling, “Analysis of simulation methodology for calculation of the heat of transport for vacancy thermodiffusion,” *J. Appl. Phys.*, vol. 116, no. 2, p. 23504, Jul. 2014.

[37] R. Krishna and J. M. van Baten, “The Darken Relation for Multicomponent Diffusion in Liquid Mixtures of Linear Alkanes: An Investigation Using Molecular Dynamics (MD) Simulations,” *Ind. Eng. Chem. Res.*, vol. 44, no. 17, pp. 6939–6947, Aug. 2005.

[38] P. Steve and S. Plimpton, “Fast parallel algorithms for short-range molecular dynamics,” *J. Comput. Phys.*, vol. 117, no. 1, pp. 1–19, 1995.

[39] M. Vijayakumar, S. Kerisit, Z. Yang, G. L. Graff, J. Liu, J. a Sears, S. D. Burton, K. M. Rosso, and J. Hu, “Combined 6,7 Li NMR and Molecular Dynamics Study of Li Diffusion in Li2TiO3,” *J. Phys. Chem. C*, vol. 113, no. 46, pp. 20108–20116, 2009.

[40] M. Matsui and M. Akaogi, “Molecular Dynamics Simulation of the Structural and Physical Properties of the Four Polymorphs of TiO 2,” *Mol. Simul.*, vol. 6, no. 4–6, pp. 239–244, May 1991.

[41] M. P. Allen and D. J. Tildesley, *Computer Simulation of Liquids*. Clarendon Press, 1989.

[42] P. K. Naicker, P. T. Cummings, H. Zhang, and J. F. Banfield, "Characterization of Titanium Dioxide Nanoparticles Using Molecular Dynamics Simulations," *J. Phys. Chem. B*, vol. 109, no. 32, pp. 15243–15249, 2005.

[43] D. R. Collins, W. Smith, N. M. Harrison, and T. R. Forester, "Molecular dynamics study of TiO2 microclusters," *J. Mater. Chem.*, vol. 6, no. 8, p. 1385, 1996.

[44] M. Matsui and M. Akaogi, "Molecular Dynamics Simulation of the Structural and Physical Properties of the Four Polymorphs of TiO2," *Mol. Simul.*, no. January 2013, pp. 37–41, 1991.

[45] P. Goel, N. Choudhury, and S. L. Chaplot, "Superionic behavior of lithium oxide <math display='inline'> <mrow> <msub> <mi mathvariant='normal'>Li</mi> <mn>2</mn> </msub> <mi mathvariant='normal'>O</mi> </mrow> </math> : A lattice dynamics and molecular dynamics study," *Phys. Rev. B*, vol. 70, no. 17, p. 174307, Nov. 2004.

[46] A. D. Mulliner, P. C. Aeberhard, P. D. Battle, W. I. F. David, and K. Refson, "Diffusion in Li_2 O studied by non-equilibrium molecular dynamics for 873 < T/K < 1603.," *Phys. Chem. Chem. Phys.*, vol. 17, no. 33, pp. 21470–5, Sep. 2015.

[47] L. S. Darken, "Diffusion, mobility and their interrelation through free energy in binary metallic systems," *Trans. Aime*, vol. 175, no. 1, pp. 184–201, 1948.

[48] J. R. Morris, C. Z. Wang, K. M. Ho, and C. T. Chan, "Melting line of aluminum from simulations of coexisting phases," *Phys. Rev. B*, vol. 49, no. 5, pp. 3109–3115, Feb. 1994.

[49] M. S. ORTMAN and E. M. LARSEN, "Preparation, Characterization, and Melting Point of High-Purity Lithium Oxide," *J. Am. Ceram. Soc.*, vol. 66, no. 9, pp. 645–648, Sep. 1983.

[50] A. V. Chadwick, K. W. Flack, J. H. Strange, and J. Harding, "Defect structures and ionic transport in lithium oxide," *Solid State Ionics*, vol. 28–30, pp. 185–188, Sep. 1988.

[51] T. W. D. Farley, W. Hayes, S. Hull, M. T. Hutchings, and M. Vrtis, "Investigation of thermally induced Li + ion disorder in Li 2 O using

neutron diffraction," *J. Phys. Condens. Matter*, vol. 3, no. 26, pp. 4761–4781, Jul. 1991.

[52] R. M. Fracchia, G. D. Barrera, N. L. Allan, T. H. K. Barron, and W. C. Mackrodt, "Lithium oxide and superionic behaviour—A study using potentials from periodic ab initio calculations," *J. Phys. Chem. Solids*, vol. 59, no. 3, pp. 435–445, Mar. 1998.

[53] M. J. O'Neil, *The Merck Index - An Encyclopedia of Chemicals, Drugs, and Biologicals*. 2013.

[54] V. Van Hoang, "The glass transition and thermodynamics of liquid and amorphous TiO(2) nanoparticles.," *Nanotechnology*, vol. 19, no. 10, p. 105706, 2008.

[55] J. L. Ethridge, D. E. Baker, and A. D. Miller, "Effects of Fast Neutron Irradiation on Thermal Conductivity of Li2O and LiAlO2," *J. Am. Ceram. Soc.*, vol. 71, no. 6, p. C-294-C-296, Jun. 1988.

[56] T. Takahashi and T. Kikuchi, "Porosity dependence on thermal diffusivity and thermal conductivity of lithium oxide Li2O from 200 to 900°C," *J. Nucl. Mater.*, vol. 91, no. 1, pp. 93–102, Jun. 1980.

[57] F. R. Charvat and W. D. Kingery, "Thermal Conductivity: XIII, Effect of Microstructure on Conductivity of Single-Phase Ceramics," *J. Am. Ceram. Soc.*, vol. 40, no. 9, pp. 306–315, 1957.

[58] R. A. HEIN, P. N. FLAGELLA, and J. B. CONWAY, "High-Temperature Enthalpy and Heat of Fusion of UO2," *J. Am. Ceram. Soc.*, vol. 51, no. 5, pp. 291–292, May 1968.

[59] J. G. Rodeja, M. Meyer, and M. Hayoun, "Derivation and validation of model potentials for Li 2 O from density-functional theory," *Model. Simul. Mater. Sci. Eng.*, vol. 9, no. 2, pp. 81–96, Mar. 2001.

[60] D. J. Evans and D. MacGowan, "Addendum to '"Heat and matter transport in binary liquid mixtures,"'" *Phys. Rev. A*, vol. 36, no. 2, pp. 948–950, Jul. 1987.

[61] Y. Ishii, K. Sato, M. Salanne, P. A. Madden, and N. Ohtori, "Thermal conductivity of molten alkali metal fluorides (LiF, NaF, KF) and their mixtures," *J. Phys. Chem. B*, vol. 118, no. 12, pp. 3385–3391, 2014.

국문초록

새로운 재료의 개발은 원자핵공학의 진보를 위해 필수적으로 수반되어야 할 일이다. 발전시켜야 할 재료의 여러가지 물성치 중에서 열전도율은 원자력발전의 안전과 직결되는 중요한 물성치로 여겨져 왔다. 재료의 정확한 열전도율을 계산하고 이를 개선시키기 위한 방법으로 여러가지 실험적인 접근이 많이 이루어져 왔다. 그러나 원자력 발전소의 실제 운영환경에 적합한 실험은 현실적으로 많은 제약이 있기 때문에 이를 보완하기 위해 계산적인 방법 또한 꾸준히 수행되어 져 왔다.

본 논문에서는 열전도율을 구하기 위한 계산적인 방법 중 하나인 평형분자동역학 (Equilibrium Molecular Dynamics) 이 이원계 (Binary systems) 물질들의 적용된 사례에서 발견된, 3 가지로 혼재하는 열전도율 표현식에 관하여 고찰하였다. 먼저 열전도율 표현식이 다양하게 존재하는 이유에 관하여 이론적으로 밝히었다. 그 결과로, κ_2 라는 열전도율 표현식이 가장 이론적으로 정확함을

확인하였다. 이를 통해 κ_2 를 기준으로 다른 열전도율 표현식의 오차 정도를 가늠하였다. 이론적인 접근을 통하여 열전도율 표현식의 오차정도는 원자 확산율와 밀접한 관련이 있음을 밝혔다.

앞서 이루어진 이론적인 고찰을 검증하기 위해 Li_2O 와 TiO_2 모델 시스템에서 평형분자동역학 시뮬레이션을 진행하였다. 원자 확산율이 열전도율 표현식의 오류정도에 미치는 영향을 검증하기 위해 Li_2O 와 TiO_2 의 무질서한 상 (비정질, 액상) 에 관한 시뮬레이션 또한 진행되었다. 그 결과로 κ_1^* 로 불리는 열전도율 표현식이 Li_2O 에서 κ_2 대비 최대 120%, TiO_2 에서 최대 60%의 오류를 가져옴을 확인하였다.

본 논문에서 이론적인 접근을 통해 일부 열전도율 표현식이 부적절한 값을 내는 이유에 관해 다음과 같이 고찰하였다. 기본적으로 열전도율은 물질이 얼마나 열을 잘 전달하는지에 관한 척도이다. 이때 적절한 표현식인 κ_2 와는 달리, 다른 두 가지의 열전도율 표현식 (κ_1 , κ_1^*)은 원자의 이동으로 인한 에너지의 수송을 열전도율로 고려하는 것이 중요한 이유로 생각되었다. κ_1 와 κ_1^* 에서 원자의 이동으로 수송되는 에너지를 제거한 표현식이 κ_2 인 것이다. 이때 원자의 이동으로 수송되는 에너지의 양은 재료에 따라 다르게 되는데 이들이 부분비 엔탈피 (partial specific

enthalpy)와 환산 수송열 (reduced heat of transport) 로 특징지어졌다. 하지만 열전도율 표현식에서 이와 같이 부적절한 열 수송량으로 간주되는 항들은 원자 확산도 중 하나인 Maxwell-Stefan 확산도가 충분히 높지 않으면 드러나지 않는 것으로 밝혀졌다.

이와 같은 일부 열전도율 표현식의 오류정도를 손쉽게 가늠하기 위해 본 논문에서는 재료의 물성치 중 비교적 손쉽게 구할 수 있는 자가 확산도 (Self diffusion coefficient)와 0 K 에서의 부분비 엔탈피 값을 활용할 것을 제안하였다. 또한 이원계 시스템 중에서 비교적 가벼운 원소를 불순물로 함유하고 있는 재료가 κ_l 이 부적절한 값을 내기 쉽기 때문에 열전도율 계산에 주의를 기울일 것을 제안하였다.